UCRL-17435

University of California

Ernest O. Lawrence Radiation Laboratory

APPLICATION OF ATOMIC BEAMS TO ELEMENTARY PARTICLE AND NUCLEAR PHYSICS

DISCLAIMER

For Annual Reviews of
Nuclear Science
Vol. 17, 1967

UCRL-17435
Preprint

UNIVERSITY OF CALIFORNIA

Lawrence Radiation Laboratory
Berkeley, California

AEC Contract No. W-7405-eng-48

APPLICATION OF ATOMIC BEAMS TO ELEMENTARY PARTICLE AND NUCLEAR PHYSICS

Eugene D. Commins

March 15, 1967

APPLICATION OF ATOMIC BEAMS TO ELEMENTARY PARTICLE AND NUCLEAR PHYSICS[1,2]

By Eugene D. Commins

Lawrence Radiation Laboratory and Department of Physics
University of California, Berkeley, California

CONTENTS

[1]The survey of literature for this review was concluded in January 1967.

[2]This review was written under the auspices of the U. S. Atomic Energy Commission.

1. INTRODUCTION

1.1 Scope of This Review

Atomic-beam experiments have provided much useful and precise information to nuclear and elementary-particle physics over the past several decades. For the purposes of this review, the significant recent developments in atomic-beam research are divided into three main categories:

1.1.1 Structure of hydrogenic atoms; tests of quantum electrodynamics. — The invention of modern covariant quantum electrodynamics followed directly from the dramatic and celebrated discoveries of the Lamb shift and the anomalous magnetic moment of the electron in the late forties. Today, precise and critical tests of quantum electrodynamics are still provided by measurements of the radio-frequency spectra of hydrogenic atoms with atomic-beams and related techniques. For example, within the past several years new determinations of the fine structure of the n = 2 states of hydrogen and deuterium have suggested the necessity for revision of the long-accepted value of the fine-structure constant α, and have yielded results for the $2^2S_{1/2} - 2^2P_{1/2}$ "Lamb shift" separation in disagreement with theory. A detailed discussion of recent work on hydrogenic atoms is given in Section 3.

1.1.2 Atomic-beam tests of symmetry and invariance principles. — The main developments described here have taken place along two distinct lines. For one, there are the recent sensitive atomic-beam tests for intrinsic static electric dipole moments (EDM) of the electron and neutron. If an elementary particle were discovered to possess a finite electric dipole moment, this would signify a breakdown of reflection and time-reversal invariance.

In another development a sensitive test of time-reversal invariance in allowed beta decay has been made by observation of the decays-in-flight of a polarized atomic beam of ^{19}Ne. These and other tests of conservation laws are considered in Section 4.

1.1.3 Static properties of atomic nuclei. —The standard atomic-beam magnetic-resonance method continues to be useful for the determination of spins, hyperfine structures (hfs), and static nuclear multipole moments. An interesting new development has been its application to the study of isotope shifts, considered in Section 5. That section also contains a brief review of the current status of magnetic moment determinations for mirror nuclei.

At certain places in this review I discuss experiments which are outside the strict domain of atomic beams. These are included where it is felt that they make the general argument more coherent and comprehensible. For lack of space, I have omitted mention of many interesting recent works in standard atomic beams. I make no pretense at completeness and apologize to my colleagues and readers for these omissions.

Applications of atomic beams to production of polarized ion and electron beams for accelerators is discussed in another chapter of this volume (Haeberli).

1.2 Other Reviews and Monographs

Several thorough and detailed expositions of atomic-beam research have been published. Notable are the monographs of Ramsey (1), and of Kusch and Hughes (2). Both treat exhaustively the standard methods and all principal developments which occurred as late as the mid-fifties. Kopfermann's book Nuclear Moments (3) covers a broader range of

material in somewhat less detail. More specialized works have also appeared, for example, the article by Hubbs and Nierenberg (4), which was published together with summaries of spin, parity, and nuclear moment determinations by optical, microwave, nuclear magnetic resonance (NMR), electron spin resonance (ESR), angular correlation, and nuclear-orientation methods. Chapters have also appeared in this series of volumes (5, 6, 7, 8, 9). A useful compilation of nuclear-moment values, obtained by various techniques, contains results which appeared in the literature before May 1964, and was prepared by Fuller and Cohen (10). A revised edition of the Fuller-Cohen table will shortly be published, and therefore we have not attempted to present a similar complete table in this review.

Because such an extensive literature exists on atomic beams and related techniques, we shall give only a very brief resume of the well-known standard methods in Part 2, mainly to provide some background for the discussions which follow.

2. STANDARD ATOMIC-BEAM METHODS

2.1 Basic Techniques

The standard atomic-beam magnetic resonance spectrometer is used to determine the energy differences between pairs of atomic levels, with corresponding frequencies ordinarily ranging from several cycles per second to hundreds of thousands of megacycles per second, and occasionally extending to the optical region. The typical atomic-beam device consists of a beam source with a beam-defining slit, one or more collimating slits, possibly one or several beam stops, a detector, two inhomogeneous magnetic fields A and B which serve as state selectors,

and between the latter, a transition region immersed in a homogeneous magnetic field C. (See Figure 1.) The spectrometer is capable of very high resolution, since linewidths are usually determined by the time spent by beam atoms in the transition region, and they are determined little or not at all by effects such as spontaneous emission, and Doppler and collision broadening. The beam is usually composed of neutral atoms which effuse from the source aperture with a Maxwellian velocity distribution $f(v) \approx v^3 \exp(- mv^2/2kT)$ characteristic of the source temperature T. Ordinarily the levels to be investigated are sublevels of the ground state or a metastable state with a mean life long compared with the beam transit time through the apparatus, although some experiments have been done on short-lived excited states (11). Atomic excitation is sometimes produced directly at the source, when, for example, a discharge tube provides a beam of noble gas atoms in a metastable state (12). Excitation can also be produced by electron bombardment or optical excitation of the beam (13, 14). Discharge tubes and high-temperature ovens dissociate molecular gases such as H_2, O_2, and Cl_2 to form atomic beams such as H and O (15, 16). Many radioactive isotopes which have special source problems (7), have been investigated in the last 10 to 15 years. In several atomic-beam experiments, a continuous and rapid flow of radioactive material was maintained from production site (a cyclotron or reactor target) to the atomic beam source (17, 18, 19).

Several standard methods of beam detection are used, including the hot-wire surface-ionization detector (20) (which is nearly 100 percent efficient for alkali atoms), the 'universal' mass spectrometer detector (21), the method of deposition of condensible radioactive beams (22), and the

method of surface ejection of electrons by metastable atoms and ions (23, 24). Alongside these well-established techniques several novel methods have been used successfully; these will be described in context below.

The inhomogeneous magnetic fields A and B spatially deflect the beam according to the well-known formula:

$$\underset{\sim}{F} = - \underset{\sim}{\nabla} W = \underset{\sim}{\nabla}(\underset{\sim}{\mu} \cdot \underset{\sim}{B}) \qquad 1.$$

Here $\underset{\sim}{F}$ is the force on the atom, $\underset{\sim}{W}$ is the internal energy of the atom, $\underset{\sim}{\mu}$ is the atomic magnetic moment, and $\underset{\sim}{B}$ is the deflecting field. In the ordinary two-wire or dipole field configuration, the beam is ribbon-shaped (see Figure 2). In this case equation 1 reduces to

$$F_z = \mu_{eff} (\partial B/\partial z) \qquad 2.$$

where $\mu_{eff} = - \partial W/\partial B$, and $\underset{\sim}{z}$ is the direction shown in Figure 2.

Extensive use has also been made of quadrupole and hexapole deflecting fields, where the beam has a circular cross section and the deflections are radial (25). (See Figure 3.)

Transitions induced in the C region are detected by their effect on the subsequent trajectory of the beam in the B region. Typically, such transitions are brought about by imposing an oscillating magnetic field applied within a well-defined transition region in addition to the homogeneous static magnetic field $\underset{\sim}{B}_0$. The latter may range from a fraction of a gauss to several thousand gauss. In the simplest case we are concerned with the probability $P_{p,q}(t)$ for a transition from level p to level q of a single atom with two levels p, q in the time $t = \ell/v$, where v is the velocity of the atom in the transition region. If the oscillating field has angular frequency ω, the matrix element coupling the two levels may be written

$$\langle q \mid \mathcal{H}' \mid p \rangle = Ve^{i\omega t}$$

and one obtains the well-known formula (26)

$$P_{p,q}(t) = \sin^2\Theta \sin^2(at/2) \qquad 3.$$

where $\sin\Theta$ equals $2b/a$, a^2 equals $(\omega-\omega_0)^2 + (2b)^2$, b equals $V/\hbar$, and $\hbar\omega_0$ is the energy difference between levels p and q. (Since the actual time dependence of the oscillating field is $\cos\omega t$ rather than $e^{i\omega t}$, there is an additional component $\propto e^{-i\omega t}$ which leads to a frequency shift (27) of order $|V|^2/\hbar\omega_0$ in the resonance.) If the levels p and q are magnetic sublevels $m = \pm 1/2$ for a particle with angular momentum $I = 1/2$, then ω_0 is the Larmor frequency γB_0 (with γ the gyromagnetic ratio) and $b = \gamma B_1/2$. For a particle with angular momentum $I > 1/2$, the transition probabilities between the magnetic substates m and m' are given by the Majorana formula (28)

$$P_{mm'} = (\sin\tfrac{x}{2})^{4I}(I+m)!(I+m')!(I-m)!(I-m')! \qquad 4.$$
$$\cdot\left\{\sum_{r=0}^{2I}{}' (-1)^r \frac{[\cot\frac{x}{2}]^{2r+m+m'}}{r!(r+m+m')!(I-m-r)!(I-m'-r)!}\right\}^2$$

where x is defined by $P_{1/2 \to 1/2} = \sin^2(x/2)$, and r is limited to those values for which all factorials are positive or zero ($0! \equiv 1$).

Frequent use is made in atomic-beam experiments of a scheme first proposed by Ramsey (29, 30), namely, that of two oscillating or rotating fields confined to regions of length ℓ at either end of the transition region (separated by length L). In this scheme one finds the single-particle transition probability for the two-level system p, q to be

$$P_{p,q} = 4\sin^2\Theta \sin^2\frac{at}{2}$$
$$\cdot\left[\cos\frac{(\lambda T-\delta)}{2}\cos\frac{at}{2} - \cos\Theta\sin\tfrac{1}{2}(\lambda T-\delta)\sin\frac{at}{2}\right]^2 \qquad 5.$$

where $t = \ell/v$, $T = L/v$, Θ is defined as before, $\lambda = \overline{\omega}_0 - \omega$ (with $\overline{\omega}_0$ the average frequency separation between levels p and q over region L), and δ is the phase difference between the two rf fields.

One of the principal advantages of the separated oscillating-field method is that field-dependent resonances are relatively insensitive to inhomogenieties in the static field B_0 in the intermediate space L. The method also lends itself to special important applications, as is shown by the following example.

Consider a beam of particles of spin $\frac{1}{2}$ (e.g., free neutrons), and suppose that the two separated oscillating fields are in phase ($\delta = 0$). Suppose in addition that the neutrons enter the first oscillating field with spin up and velocity v, and that the first rf field is at the resonance frequency ω_0 and is just strong enough to tip the polarization vector from the z direction into the xy plane. In the region L between the separated oscillating fields, the polarization vector precesses in the xy plane. The total precession angle ϕ accumulated between separated oscillating fields is given by

$$\phi = \int_0^{L/v} \gamma B_0(x)dt = \frac{\gamma}{v}\int_0^{L} B_0(x)dx = \frac{\gamma}{v}\,\overline{B_0 L} = \overline{\omega}_0\,\frac{L}{v}$$

If $\overline{\omega}_0 = \omega_0$, the particle is in phase with the second rf field and is tipped downward through another 90 degrees; eventually the particle has flipped 180 degrees (spin down). However, if in the space between the separated oscillating fields, one introduces an external perturbation which modifies the rate at which ϕ increases, the particle is no longer in phase with the second rf field, and a total 180 degree flip no longer results. Such a perturbation would arise if the neutron possessed an electric dipole

moment, and if one introduced an external electric field into the space between separated oscillating fields.

The total transition probability for a beam with a velocity distribution $f(v)$ is obtained by averaging the appropriate single-particle probability over $f(v)$. When $f(v)$ is the standard Maxwellian distribution, one may compute the total transition probability from tables (31). A typical resonance for separated oscillating fields and for a beam with a Maxwellian distribution is shown in Figure 4.

2.2 Spins, Nuclear Moments, and Hyperfine Structures

That part of the atomic Hamiltonian which is relevant to atomic-beam magnetic resonance investigations concerns the hyperfine structure and Zeeman effect:

$$\mathcal{H} = \mu_0 \, g_J \, \underset{\sim}{J} \cdot \underset{\sim}{B}_0 + \mu_0 \, g_I \, \underset{\sim}{I} \cdot \underset{\sim}{B}_0 + \sum_{\ell} \underset{\sim}{T}^{\ell}_M(r_e) \cdot \underset{\sim}{T}^{\ell}_M(r_N) + \sum_{\ell} \underset{\sim}{T}^{\ell}_E(r_e) \cdot \underset{\sim}{T}^{\ell}_E(r_N) \qquad 6.$$

Here the first and second terms correspond to the interaction of the electronic and nuclear magnetic dipole moments, respectively, with an external magnetic field $\underset{\sim}{B}_0$. The sign convention is chosen to give $g_J > 0$, with the Bohr magneton $\mu_0 > 0$. The third term gives the hyperfine interaction of various magnetic multipole moments of the electronic current distribution with the corresponding nuclear magnetic multipole moments. Inversion symmetry requires that the expectation values of all terms with even ℓ in this sum be zero. The fourth term on the right-hand side of Equation 6 represents the electric hyperfine interaction in various multipole orders, with the restriction that the expectation values of all odd ℓ terms be zero, again from inversion symmetry. The expectation values

of all terms in both sums must of course be zero for $\underline{\ell} > 2I$ or $\underline{\ell} > 2\underline{J}$.

In most cases, only M1 (magnetic dipole) and E2 (electric quadrupole) hyperfine interactions are significant, M3 (magnetic octupole) interactions having been observed only in isolated cases (32).

The magnetic dipole hfs term can be written as

$$\mathcal{H}_{M1} = ha\, \underset{\sim}{I} \cdot \underset{\sim}{J} \qquad 7.$$

This term causes a given atomic state to be split into $2n+1$ hfs levels, where $\underline{n}$ is $\underline{I}$ or $\underline{J}$, whichever is smaller. For a state with no electric quadrupole hfs interaction, the hfs splittings between the successive levels $\underline{F} = \underline{I} + \underline{J}$, $\underline{I} + \underline{J}-1$, $\underline{I} + \underline{J}-2$, $\cdots$ are equal to $(\underline{I} + \underline{J})ha$, $(\underline{I} + \underline{J}-1)ha \cdots$, respectively.

The magnetic dipole interaction constant $\underline{a}$ is given by

$$a = \frac{\mu_I \langle B(0) \rangle}{h\,IJ} \qquad 8.$$

where μ_I is the nuclear magnetic moment, and $\langle B(0) \rangle$ is the average magnetic field at the nucleus due to the electron distribution. To determine μ_I directly from $\underline{a}$, one must know the atomic wave function accurately, in order to compute $\langle B(0) \rangle$. For hydrogenic atoms in s states, ha is given by the Fermi formula (33) corrected with several small but important factors. Formulae for ha in non-S states in hydrogen, and approximate formulae for ha in other atoms, are discussed by Ramsey (34), Kusch and Hughes (35), and Kopfermann (36).

If the nuclear magnetic dipole moment μ_1 and hfs splitting $\Delta\nu_1$ are known for one isotope with spin I_1, then knowledge of $\Delta\nu_2$ for a second isotope permits determination of μ_2 through the formula

$$\frac{\mu_1}{\mu_2} = \frac{2I_2+1}{I_2}\,\frac{I_1}{2I_1+1}\,\frac{\Delta\nu_1}{\Delta\nu_2} \qquad 9.$$

within the restrictions imposed by the existence, in many cases, of a hyperfine structure anomaly $_2\Delta_1$ defined by

$$(1 - {}_2\Delta_1) = \left(\frac{\Delta\nu_1}{\Delta\nu_2}\right)\left(\frac{\mu_2}{\mu_1}\right)\left(\frac{I_1}{2I_1+1}\right)\left(\frac{2I_2+1}{I_2}\right)\left(\frac{M_2}{M_1}\right)^3 \qquad 10.$$

The hfs anomaly may be as large as $\approx 1\%$ (37, 38, 39). (See Section 3.1.5 for a discussion of hyperfine anomalies in the isotopes of hydrogen.)

The electric quadrupole term in the Hamiltonian is

$$\mathcal{H}_{E2} = hb\,\frac{\left[3(\underline{I}\cdot\underline{J})^2 + \frac{3}{2}\,\underline{I}\cdot\underline{J} - \underline{I}^2\underline{J}^2\right]}{2I(2I-1)\,J(2J-1)} \qquad 11.$$

where $\underline{b}$ (the electric quadrupole hfs interaction constant) is given in terms of $\underline{Q}$ (the nuclear quadrupole moment) and $\partial E/\partial z$ (the derivative of the electric field at the nucleus arising from the electronic distribution) as $(e/h)Q(\partial E/\partial z)$. To obtain $\underline{Q}$ from $\underline{b}$, one must estimate $\partial E/\partial z$ from the atomic wave function. This is complicated by the fact that the nuclear quadrupole moment may cause a polarization of the atomic "core" electrons (Sternheimer effect) (40).

For $J = \frac{1}{2}$ or $I = \frac{1}{2}$, the term $\mathcal{H}_{E2}$ does not contribute to the total energy. For these important special cases, the secular equation is quadratic and may be solved explicitly to yield the well-known Breit-Rabi formula for the energy of the atom in an arbitrary (41) external magnetic field B_0. For $J = \frac{1}{2}$,

$$W = -\frac{\Delta W}{2(2I+1)} + \mu_0 g_I B_0 m \pm \frac{\Delta W}{2}\left[1 + \frac{4mx}{2I+1} + x^2\right]^{1/2} \qquad 12.$$

where $\Delta W = h\Delta\nu = (I+\frac{1}{2})ha$ is the zero-field splitting between the states $F = I+\frac{1}{2}$ and $F = I-\frac{1}{2}$, and $x = (g_J - g_I)\,\mu_0 B_0/\Delta W$. The $\pm$ sign corresponds to $F = I \pm \frac{1}{2}$, respectively.

For $I = \frac{1}{2}$, one obtains an analogous formula by interchanging I and J wherever they occur in Equation 12.

Figures 5 and 6 are typical energy-level diagrams for $I = 1/2$, $J = 1/2$, and $I = 7/2$, $J = 1/2$, respectively. The transitions a, b, c, d and e shown in Figure 6 are illustrative of the procedures commonly employed in atomic-beam magnetic resonance work to extract information about the atomic nucleus. Each transition takes place between levels which have nearly opposite high-field magnetic moments, and therefore each transition can cause an observable change in the beam deflection pattern. Transition a, which takes place at very low field, has a frequency depending significantly only on B_0 and I, and therefore leads to determination of the spin. Transition b between the same pair of levels has a frequency depending on $\Delta\nu$ as well as B_0 and I, and therefore can be used to determine $\Delta\nu$ with moderate accuracy. Transition c at low external field is independent of B_0 to first order and can be used to determine $\Delta\nu$ to very great accuracy. Transitions d and e have frequency minima at $x = + |m_F|/2I+1$, $(m_F < 0)$, for which

$$W(F=4, m_F) - W(F=3, m_F) = 2|m_F| g_I \mu_0 B_0 .$$

These transitions result in sharp resonance lines and can be used to determine g_I directly, if B_0 is known independently. This is the best general method for precise determination of nuclear magnetic moments in atomic beams work.

For $I > \frac{1}{2}$, $J > \frac{1}{2}$, the secular equation is of third degree or higher, an electric quadrupole term may contribute to the energy, and in general the Hamiltonian must be diagonalized by approximation methods. Useful formulae for matrix elements and detailed calculations are given by

Ramsey (42) and Kusch and Hughes (43).

3. RADIO-FREQUENCY SPECTRA OF HYDROGENIC ATOMS. TESTS OF QUANTUM ELECTRODYNAMICS

3. Hyperfine Structure

To date the ground-state hfs separations of positronium, muonium, hydrogen, deuterium, tritium, and singly ionized helium-3, and the hfs separations in the $2^2S_{1/2}$ states of H, D, and $^3_2He^+$ have been determined by atomic-beam and related methods (see Table I). In this section we shall discuss these measurements and their principal implications. Experimental details will be presented only where new atomic-beam techniques are involved or where special questions arise.

3.1.1 Positronium. — The ground-state hfs Hamiltonian for positronium contains, in addition to the spin-spin interaction, a sizable contribution arising from pair annihilation effects (44). In lowest order (α^2) this contributes about 40% to $\Delta\nu$. The experimental results (obtained by microwave-counting methods) are in good agreement with theory, not only to lowest order, but also to next order (α^3) (45, 46). The precision is not high enough to yield a value of α comparable to those obtained from other experiments.

3.1.2 Muonium. —Great interest exists in the precise determination of the hfs splitting of muonium. Since the muon is a lepton, the theoretical formula for $\Delta\nu$ contains no uncertain nucleon structure terms and may be compared directly with experiment to yield a value for α. [See Hughes (47).] Starting with the theoretical formula for $\Delta\nu$, one readily arrives at the following expression:

$$\Delta\nu(\mu^+e^-, 1^2S_{1/2}) = 2.632\,936\times10^7\,\alpha^2(\mu_\mu/\mu_p)\ \text{MHz} \qquad 13.$$

TABLE I

Hfs of Hydrogenic Atoms

Atom		Electronic state	Hfs interval	$\Delta\nu$ Experimental (MHz)	Method	Reference
Positronium	e^+e^-	S	$^3S_1$-$^1S_0$	$(2.0335 \pm 0.0004)\times 10^5$	Microwave-counting	a
Muonium	μ^+e^-	$1^2S_{1/2}$	F=1 : F=0	4463.16 ± 0.06	Microwave-counting	b
Hydrogen	^1_1H	$1^2S_{1/2}$	F=1 : F=0	1420.405751800(28)	H maser	c
Hydrogen	^1_1H	$2^2S_{1/2}$	F=1 : F=0	177.55686(5)	ABMR[j]	d
Deuterium	^2_1H	$1^2S_{1/2}$	$F=\frac{3}{2} : F=\frac{1}{2}$	327.384325(5)	H maser	e
Deuterium	^2_1H	$2^2S_{1/2}$	$F=\frac{3}{2} : F=\frac{1}{2}$	40.924439(20)	ABMR	f
Tritium	^3_1H	$1^2S_{1/2}$	F=1 : F=0	1516.70170(7)	ABMR	g
$^3_2He^+$		$^2S_{1/2}$	F=0 : F=1	8665.649905(50)	Ion trap	h
$^3_2He^+$		$2^2S_{1/2}$	F=0 : F=1	1083.35499(20)	Ion beam	i

[a] References 44, 45, 46

[b] References 47, 48, 49

[c] Reference 50

[d] Reference 51

[e] Reference 52

[f] Reference 53

[g] Reference 54

[h] Reference 55

[i] Reference 56

[j] Atomic-beam magnetic resonance

To obtain $\underline{a}$ one requires the experimental values of $\Delta\nu$ (48, 49), and μ_μ/μ_p, the ratio of the muon's magnetic moment to the proton's magnetic moment. This latter quantity has been measured by Hutchinson et al. (57). In the work of these authors, positive muons were stopped in H_2O or HCl targets and allowed to precess in a static longitudinal magnetic field and a variable-frequency pulsed rf magnetic field. Magnetic resonances were observed by detecting changes in the angular distribution of electrons emitted in muon decay.

One must ask to what extent the magnetic field at the muon is affected by its chemical environment (diamagnetic correction). Ruderman (58) has shown that the diamagnetic correction for the muon in H_2O might be as little as 10 ppm or even less, rather than 26 ppm, as was assumed by Hutchinson et al.

In the absence of some independent method for determining μ_μ/μ_p, we assume that the diamagnetic correction is 13±13 ppm, from which one finds

$$a^{-1} = 137.0379 \pm 0.0021 \qquad 14.$$

Obviously another direct and precise determination of μ_μ would be extremely valuable, since the diamagnetic correction is the weakest link in the chain leading from $\Delta\nu$ to $\underline{a}$. (A summary of the current situation as regards $\underline{a}$ is given in Section 3.3).

3.1.3 The hydrogen ground state. —The hfs of the ground states of hydrogen and deuterium have been determined to remarkable precision with the hydrogen maser, an atomic-beam device invented by Kleppner, Ramsey, and co-workers at Harvard in 1960 (15, 50, 52, 59, 60), and since used by them in a series of very beautiful and accurate experiments. The

maser functions as follows: A beam of atomic hydrogen is formed by dissociating H_2 in a discharge. (See Figure 7.) The beam is transmitted through a hexapole deflecting magnet which focuses atoms in the states $m_I = \frac{1}{2}$, $m_J = \frac{1}{2}$, and $m_I = -\frac{1}{2}$, $m_J = \frac{1}{2}$ toward the center axis. (See Figure 4.) The focused portion of the beam enters a glass bulb through a narrow channel, where the atoms remain for an average time $t = V/S$; here V is the bulb volume and S is the conductance of the channel for molecular flow. The bulb is in a high-Q microwave cavity designed to operate in the TE_{011} mode at the hfs resonance frequency, and the cavity and bulb are immersed in a weak homogeneous magnetic field. The time t is of order 1 second, during which the atoms in the bulb collide with the wall about 10^5 times. However, relaxation of polarization is prevented by coating the bulb's inner wall with a thin layer of Teflon (61). Consequently, the effective radiative lifetime is $t \approx 1$ sec for maser oscillations which occur when atomic transitions ($F = 1$, $m_F = 0 \longleftrightarrow F = 0$, $m_F = 0$) are resonance-coupled to the cavity. The narrow linewidths thus achieved make possible a remarkably precise determination of $\Delta\nu$. A number of small effects which might contribute to relaxation of polarization or shifts in resonance frequency have been investigated carefully. These include spin-exchange collisions between atoms in the bulb, depolarization of atoms arising from their motion through a slightly inhomogeneous magnetic field, frequency shifts due to wall collisions, mistuning of the cavity, and a second-order Doppler shift arising from the finite velocity of the atoms in the bulb. The resonance frequency is determined by comparing it with a secondary Cs atomic-beam frequency standard, and a small Zeeman correction is applied to the observed frequency

to obtain $\Delta\nu$. These measurements are among the most precise in all of science, and they agree with earlier and less accurate determinations of $\Delta\nu$ made with standard atomic-beam (62), paramagnetic-resonance (63), and optical-pumping (64) techniques.

In a related experiment, an absolute determination of the g value of the free proton was made (65). Essentially, Myant et al. used the same type of apparatus as described above, except that the bulb and cavity were placed in a very homogeneous 3500-gauss magnetic field, and an rf coupling loop was introduced to stimulate the transitions ($F = 1$, $m_F = 1 \longleftrightarrow F = 1$, $m_F = 0$) while maser oscillations occurred simultaneously. A low-frequency resonance could be detected by its effect on the level of maser oscillation. The primary result is in terms of the electron g-value g_s:

$$g_s/g_p = 658.21049(20) \qquad 15.$$

Using the value for g_s obtained by Wilkinson and Crane (66), one obtains

$$g_p = 0.0030420652(9) \qquad 16.$$

3.1.4 Interpretation of hydrogen ground-state hfs. —The theoretical expression for the ground-state hydrogen hfs is

$$\Delta\nu\left({}^1_1\mathrm{H},\ 1^2S_{1/2}\right) = \left[\frac{16}{3}\alpha^2 R_\infty c\,\frac{g_p}{g_s}\right]\left(\frac{\mu_e}{\mu_0}\right)^2\left(1+\frac{m}{M}\right)^{-3}(1+\epsilon_1+\epsilon_2)(1-\delta_1-\delta_2) \qquad 17.$$

The factor in brackets on the right-hand side of Equation 17 includes g_p/g_s, now given by Equation 15. The second factor is the square of the ratio of the electron-spin magnetic moment to the Bohr magneton, given by Wilkinson and Crane (66) as $\mu_e/\mu_0 = 1.001159622(27)$. The third factor is the reduced mass correction (67). The fourth factor includes $\epsilon_1 = -(1-\ln 2)\alpha^2$, which is the sum of the Breit relativistic correction (68) and the Kroll-Pollack electrodynamic correction (69); and ϵ_2, a higher order electrodynamic

correction computed by Zwanziger (70) and Layzer (71). Finally, δ_1 is a correction for proton recoil (72, 73), and δ_2 is a correction for proton structure. Estimates of the structure correction δ_2 are subject to some uncertainty. As Iddings (74) and others have shown, δ_2 may be related to an integral over cross sections for electron-proton scattering by means of dispersion relations. These cross sections have not been measured and are not likely to be in the near future, since the relevant experiments involve scattering of polarized electrons by polarized protons, for which the final momentum of the electrons must be determined. However, estimates by Iddings and others (75) indicate that δ_2 is probably only several parts per million, and that $\delta_1 + \delta_2 = 35 \pm 3 \times 10^{-6}$. Assuming this is true, and using the accepted experimental values (76) of $\Delta\nu$, R_∞, c, and m/M in Equation 17, one obtains

$$a^{-1} = 137.0359 \pm 0.0008 \qquad 18.$$

Clearly the weak point in this determination of a from $\Delta\nu({}_1H^1, 1^2S_{1/2})$ is the uncertain proton-structure correction.

3.1.5 Deuterium, tritium, and singly ionized helium-three. —In comparing the hfs splittings of deuterium and tritium with that of hydrogen, we find it useful to introduce the hfs anomaly ${}_2\Delta_1$ defined by Equation 10. The large H-D anomaly ${}_H\Delta_D = -170$ppm was first explained qualitatively by A. Bohr (77). The electron motion in ${}_1H^2$ is centered about the proton. To first approximation the nucleons remain stationary during the time the much faster electron makes a "close pass," when the magnetic dipole interaction is large. However, the relative positions of electron and neutron are uncorrelated for successive "passes," so the effect of the neutron's magnetic moment on the hfs interaction is reduced. A detailed calculation (78)

of the H-D anomaly yields results which are not in very satisfactory agreement with experiment, however.

For tritium there are two neutrons with spins opposed, and the hfs anomaly is therefore extremely small, as expected (79). For $^3_2He^+$ a similar consideration applies as for deuterium—there is one odd neutron; but here the electron centers its motion about two "fixed" protons. A comparison of $\Delta\nu(^3_2He^+, 1^2S_{1/2})$ or $\Delta\nu(^3_2He^+, 2^2S_{1/2})$ with theoretical values for a point dipole ^{3}He nucleus, including all known reduced mass, electrodynamic, and relativistic corrections, yields a 186-ppm "anomaly," presumed to be due primarily to the above-mentioned nuclear structure effect (55, 56).

3.1.6 Ion spectroscopy and $^3He^+$. — The standard atomic-beam technique is obviously unsuitable for measuring the hfs of ions, including $^3_2He^+$, because it is impossible to select atomic spin states by utilizing differential deflections of well-collimated beams of charged particles. This is because these deflections depend on the orientation of magnetic dipole moments in an inhomogeneous magnetic field, when the ions are also subject to large Lorentz forces in this field. However, for $^3_2He^+$ special techniques have been applied successfully. A decade ago Novick and Commins (56) determined $\Delta\nu(^3_2He^+, 2^2S_{1/2})$ by an ion-beam method. More recently Dehmelt (80, 55) has devised an ingenious technique utilizing ion trapping to obtain a very precise determination of $\Delta\nu(^3_2He^+, 1^2S_{1/2})$. In the Dehmelt experiment (see Figure 8), $^3He^+$ ions are formed by electron bombardment of ^{3}He gas (partial pressure $\approx 10^{-9}$ torr) with a pulsed electron beam. The ions are confined in a radio-frequency "quadrupole trap" bounded by electrodes whose surfaces are hyperboloids of revolution formed to give a potential

$$\phi = (U - V_0 \cos 2\pi\nu t)\left(\frac{x^2 + y^2 - 2z^2}{2r_0^2}\right).$$

The motion of ions in the potential ϕ is described by differential equations somewhat similar to those found in the theory of strong focusing. Through appropriate choice of parameters U, V_0, and ν, it would be possible to confine ions indefinitely in the central space between the electrodes, were it not for collisions between ions and background gas. In fact, the ions gain energy from the rf field through randomizing collisions with gas atoms and are thus eventually driven to the electrodes. Dehmelt and his collaborators have nevertheless succeeded in achieving very long confinement times ($\tau \approx 20$ minutes!) for He^+ ions (81). The $^3He^+$ is oriented by spin-exchange collisions with an incident beam of Cs atoms, themselves oriented by optical pumping. The $^3He^+$ orientation is monitored by its effect on the ion confinement time; this is possible because He^+ ions are also neutralized by spin-dependent charge-exchange collisions with Cs. Changes in $^3He^+$ orientation which occur on application of an external rf signal at the hfs transition frequency are thus observed. The precision achieved thus far seems to be limited by the transverse Doppler effect ($\approx v^2/c^2$) associated with the kinetic energy of the ions. This energy may be reduced considerably if the radiation emitted by the ions in their accelerated motion is absorbed by the trap rf circuit and dissipated in an external cooled resistor. In this manner one hopes to bring the ions into thermal equilibrium with an external bath at a very low temperature. The Dehmelt trapping technique might have considerable significance as a general tool for precision rf spectroscopy of ions.

3.1.7 Interpretation of $2^2S_{1/2}$ hfs measurements. — Determinations of $\Delta\nu(2^2S_{1/2})$ as well as $\Delta\nu(1^2S_{1/2})$ for hydrogenic atoms are useful because the troublesome nucleon and nuclear-structure corrections cancel to high order in the ratio $[\Delta\nu(2^2S_{1/2})]/[\Delta\nu(1^2S_{1/2})]$, for H, D and $^3He^+$, thus making possible a comparison of experiment with quantum electrodynamics to orders α^3 and $\alpha^2 m/M$. Very good agreement between experiment and theory is found for H, D, and $^3He^+$. The theoretical calculations have been performed by Zwanziger (82) and Sternheim (83). (See Table II.) Goldwire (84) has pointed out a slight error in a previous calculation of $R(^3He^+)$, and has thus removed a very small discrepancy previously thought to exist between R_{theor} and R_{exp} for $^3He^+$.

3.2 Fine Structure

3.2.1 The Lamb shift. — The measurements of Lamb and coworkers (85-89) on the fine structure of the n = 2 states of hydrogen and deuterium, and of Lipworth and Novick (90) on the n = 2 state of $^4_2He^+$ have long been the results with which theoretical calculations of the Lamb shift are compared. (See Table III.) In addition, the measurement by Dayhoff, Triebwasser, and Lamb (DTL) (89) of the $2^2P_{3/2} - 2^2P_{1/2}$ fine-structure separation of deuterium for years provided the accepted value of α. In these experiments, atoms of H, D, and $^4_2He^+$ were formed in the $2^2S_{1/2}$ state in an external magnetic field by electron bombardment, and microwave transitions were induced to the short-lived 2P states, thereby decreasing the population of metastables. (The relevant levels are shown in Figure 9, where hfs is neglected.) In the H and D experiments, transitions (αe) and (αf) were observed, to determine the Lamb shift, and transitions (αa) and (αb) were used to measure the $2^2S_{1/2} - 2^2P_{3/2}$ splitting in deuterium. For $^4He^+$, only (αe) transitions were observed.

TABLE II

Comparison of Experimental and Theoretical

Value of $R = \left(\frac{8\Delta\nu(2^2S_{1/2})}{\Delta\nu(1^2S_{1/2})} - 1 \right)$

	Theoretical R ($\times 10^{-6}$)	Experimental R ($\times 10^{-6}$)
H	34.45(02)	34.495(060)
D	34.53(02)	34.2 (.6)
T	34.46(02)	
$^3He^+$	137.21(03)	137.33 (.19)

TABLE III

Fine Structure of Hydrogenic Atoms

Atom	Principal quantum number	Interval	Experimental f s splitting (MHz)	Experimental method	Theoretical f s splitting (MHz)
$_1H^1$	n = 2	$2^2S_{1/2}-2^2P_{1/2}$	1057.77(.10)[a]	A. B. microwave	1057.499(0.11)[k]
			1058.07(.10)[b]	A. B. level crossing	
	n = 3	$3^2S_{1/2}-3^2P_{1/2}$	313.6(5.7)[c]	A. B. microwave	314.690(.047)[l]
$_1^2H$	n = 2	$2^2S_{1/2}-2^2P_{1/2}$	1059.00(.10)[a]	A. B. microwave	1058.763(0.17)[k]
			1059.34(.10)[e]	A. B. level crossing	
		$2^2P_{3/2}-2^2S_{1/2}$	9912.59(.10)[d]	A. B. microwave	See Eq. 19
	n = 3	$3^2S_{1/2}-3^2P_{1/2}$	315.30(.80)[f]	Microwave-optical	315.34[f]
	n = 4	$4^2S_{1/2}-4^2P_{1/2}$	133(10)[f]	Microwave-optical	133[f]
$_2^4He^+$	n = 2	$2^2S_{1/2}-2^2P_{1/2}$	14040.2(4.5)[g]	Microwave-optical	14038.17(4.4)[k]
	n = 3	$3^2S_{1/2}-3^2P_{1/2}$	4183(20)[h]	Microwave-optical	4183[h]
	n = 4	$4^2S_{1/2}-4^2P_{1/2}$	1765(20)[i]	Microwave-optical	1769[i]
		$4^2P_{3/2}-4^2S_{1/2}$	20177(30)[i]	Microwave-optical	20177[i]
$_3^6Li^{++}$	n = 2	$2^2S_{1/2}-2^2P_{1/2}$	62300(1000?)[j]	Van de Graaf	62800[j]

[a] Reference 88
[b] References 91, 92
[c] Reference 95
[d] Reference 89
[e] Reference 93
[f] Reference 96
[g] Reference 90
[h] Reference 98
[i] Reference 99
[j] Reference 100
[k] Reference 94
[l] Reference 97

These experiments are notoriously difficult, chiefly because of the large resonance linewidths encountered (the natural breadth of the 2P state is 100 MHz for H and D, and 1600 MHz for He^+). Thus to achieve a precision of 100 ppm, which is required to make a critical comparison between experimental values and theoretical predictions of the Lamb shift, one must measure the resonance line center to ≈ 0.001 of its width. For this, a detailed theory of the resonance line shape is required, together with a correct account of the many subtle effects of external electric and magnetic fields on the resonance. In the original Lamb experiments, a further serious complication for H and D arose because various hfs components were only partially resolved. It was therefore necessary to make a theoretical correction for the overlap.

In the more recent work of Robiscoe (91, 92, 93), transitions from individual hfs components of the β levels of H and D are observed, and level crossing (Stark mixing with an external dc field) rather than an external microwave field effect them. The experimental arrangement is shown in Figure 10. The main components are: (a) an oven beam source at 3000°K, at which temperature H_2 is 96 percent dissociated; (b) a magnetic field (B_1 = 575 gauss) containing an electron bombardment exciter for producing $2^2S_{1/2}$ metastable atoms; (c) a weak "flopping" magnetic field B_2 generated by a well-shielded solenoid; (d) a "quenching" magnetic field B_3 generated by a pair of Helmholz coils in which the current is carefully stabilized; (e) a pair of electric field plates located at the center of the region between the Helmholz coils; and (f) a metastable atom electron-ejection detector. The function of the various components is clarified by Figure 11, which shows the Zeeman effect of the fs and

hfs of the n = 2 levels of $^{1}_{1}H$. The goal is to determine the level crossing points A and B (corresponding to $\Delta m_I=0$ transitions) and from this and the theory of the Zeeman effect, to obtain the zero field splitting.

In the experiment to determine crossing point B, metastable 2s atoms in $\underline{\alpha}$ and $\underline{\beta}$ levels are produced by electron bombardment, but only α's survive the flight through B_1. The betas decay rapidly by Stark quenching in the motional electric field $\underset{\sim}{v}x\underset{\sim}{B}/c$ since for $B_1 \approx 575$ gauss the energy difference between $\underline{\beta}$ and $\underline{e}$ is ≈ 0. Between B_1 and B_2 the field falls to zero, then reverses slightly at B_2, causing nonadiabatic transitions which rearrange the $\underline{\alpha}$ states from B_1 approximately equally in the two $\underline{\alpha}$ levels and the β_B level. There is virtually no β_A component in the beam as it enters B_3; the β_A's are not created by the nonadiabatic transitions, owing to the finite zero field $2^2S_{1/2}$ hfs splitting.

The quenching electric field applied at the center of B_3 causes Stark mixing of β_B and e_B levels ($\Delta m_I=0$), and the degree of β_B quenching is varied by changing B_3. In effect, this varies the energy denominator in the expression for Stark mixing of β_B-e_B components by the electric field. A typical resonance curve is shown in Figure 12. Crossing point A was determined in a fashion similar to B, except that in place of the small reversed field B_2 there is a weak magnetic field ($\approx$3 G) in the same direction as B_1, and provision is made for inducing rf transitions from the $\underline{\alpha}$ state ($m_F=0$) to the β_A state. The β_A-β_B purity ratio is greater than 1500 to 1. Typically the same good agreement between experimental points and calculated resonance line shape was achieved for both A and B resonances. The result for crossing point A is: S_A = 1058.05(10) MHz, and for crossing point B is S_B = 1058.07(10) MHz.

The combination of these two values is entered in Table III.

Recently Soto (94) calculated fourth-order radiative corrections to the Lamb shift which were previously estimated. These theoretical values (of Soto) are included in Table III. Clearly, serious disagreement exists between theory and experiment for the Lamb shift in H and D, n = 2. As no explanation for these discrepancies exists, there is much interest in other measurements of the Lamb shift, especially for the higher states n = 3, 4, etc., and also for hydrogenic atoms other than H, D, and He^+. Recently Lea, Leventhal, and Lamb (98, 99) have reported observations of the fs splitting in the n = 3 and 4 states of He^+, using a microwave-optical technique. Fan and co-workers (100) have also made preliminary measurements of the Lamb shift in a high-energy beam of $^6Li^{++}$ generated with a Van de Graaf accelerator. There is good reason to think that the He^+ measurements could be refined to yield results with a precision of 100 ppm; for this precision they might test the theory as well as any existing results. As for Li^{++} and other multiply-charged hydrogenic ions, it is hoped that Lamb-shift measurements will be sufficiently refined to allow critical examination of the Z dependence of various terms in the theoretical expression for the Lamb shift, although it appears difficult to achieve very high precision in these experiments.

3.2.2 The fine-structure constant. —As we have already mentioned, the accepted value of the fs constant α was for many years given by the DTL measurement of the $2^2P_{3/2}$-$2^2P_{1/2}$ separation in deuterium (89). The theoretical formula for this separation is

$$\Delta E = \frac{\alpha^2}{16} R_\infty c \left(1 + \frac{m}{M}\right)^{-3} \left\{2 \frac{\mu_e}{\mu_0} \frac{M+m}{M} - 1 + \frac{5}{8}\alpha^2 - \frac{2\alpha^3}{\pi} \ln \frac{1}{\alpha}\right\} \qquad 19.$$

Inserting the measured frequency separation of $\Delta E = 10971.58 \pm 0.10$ MHz and the accepted values of the other constants into Equation 19, one finds

$$\alpha^{-1} = 137.0388 \pm 0.0006 \qquad 20.$$

Now, ΔE is determined experimentally from the Lamb shift $2^2S_{1/2}$-$2^2P_{1/2}$ separation $\underline{S}$, and the "high-frequency" $2^2P_{3/2}$-$2^2S_{1/2}$ separation ΔE-S:

$$\Delta E = (\Delta E - S) + S .$$

Robiscoe has obtained for $\underline{S}$ a value which is larger than that obtained by DTL (89). If we make the arbitrary assumption that Robiscoe's value of $\underline{S}$ is correct, while the old DTL value of ΔE-S is still correct, we obtain a new value of ΔE and consequently a new value of $\underline{\alpha}$:

$$\alpha^{-1} = 137.0370 \pm 0.0006 \qquad 21.$$

However, it is quite obvious that no honest revision can be made on this basis, and it is urgent that the ΔE-S transition be carefully remeasured with the level crossing method.

Still another, and the most precise, result for $\underline{\alpha}$ is obtained by determination of $2e/h$ from the A. C. Josephson effect (101). From this measurement and knowledge of other fundamental constants (76), one concludes that $\underline{\alpha}$ is given by

$$\alpha^{-1} = 137.0359 \pm 0.0004 \qquad 22.$$

Let us then summarize the existing values of $\underline{\alpha}$ as follows:

$\alpha^{-1} = 137.0388 \pm 0.0006$	ΔE_{DTL}	20.
$\alpha^{-1} = 137.0379 \pm 0.0021$	muonium	14.
$\alpha^{-1} = 137.0370 \pm 0.0006$	DTL+Robiscoe	21.
$\alpha^{-1} = 137.0359 \pm 0.0004$	Josephson	22.
$\alpha^{-1} = 137.0359 \pm 0.0008$	$\Delta\nu_H$	18.

It is clear that these numbers are not consistent, and that further work remains to be done on the hydrogen fs measurements, the muon's magnetic moment, and the proton structure correction to the ground-state hydrogen hfs, before we can be satisfied that $\underline{a}$ is known to within 5 ppm.

Another possibility for a very precise determination of $\underline{a}$, discussed by Schwartz (102), consists of measuring the fine structure of the 2^3P state of ^4He by an atomic-beam magnetic resonance method (103), and using the data as input for a calculation of $\underline{a}$ based on the best available 2^3P helium wavefunction. The basis for this program is twofold: one, the comparatively narrow linewidths which are attainable (the mean life of the 2^3P state is $\tau \approx 10^{-7}$ sec as compared with $\tau = 1.6\times10^{-9}$ sec for 2P, hydrogen); and two, the possibility of constructing accurate variational two-electron wave functions with the aid of modern computers. In the experiment of Pichanick et al., (103), the beam is of spin-polarized helium atoms in the $^3S_1$ state. A helium discharge lamp excites the 2^3S_1-2^3P transition in the $\underline{C}$ field. Magnetic resonance transitions within the 2^3P state are induced during its short lifetime and are manifested by a change in magnetic quantum number m_j of the 2^3S_1 state to which the 2^3P atoms decay, and thus a change of trajectory in the $\underline{B}$ field. The result to date is

$$E(^3P_2\text{-}^3P_1) = 2291.194\pm0.008 \text{ MHz}.$$

To achieve the goal of computing $\underline{a}$, one must still measure precisely the much larger 2^3P_1-2^3P_0 splitting.

3.3 Two-Quantum Decay of the Metastable $2^2S_{1/2}$ State of He^+

Observations of the two-photon emission which accompanies the decay of the $2^2S_{1/2}$ state of He^+ in a field-free region have been reported by Lipeles, Novick, and Tolk (104). The transition rate was first calculated by Breit and Teller (105). Subsequently, the photon energy distribution was discussed by Spitzer and Greenstein (106), and the Breit-Teller computations improved by Breit and Shapiro (107).

The decay is predicted to proceed at the rate $\gamma = 8.226\, Z^6\ \text{sec}^{-1}$ (where $Z = 1$ for H, two for He^+, etc.). The photons have a continuous energy spectrum, the energy sum being of course equal to $E_{2S}-E_{1S}$. Also one expects the coincidence counting rate for the two photons to vary as $1 + \cos^2\theta$, where θ is the angle between the directions of emission of photons 1 and 2.

In the work of Lipeles, Novick, and Tolk, the spectrum, decay rate, and angular correlation were verified by observation of the decays-in-flight of a beam of $2^2S_{1/2}$ He^+ ions with 12-eV kinetic energy. The measurements are of interest as the first experimental observations of such a two-photon spontaneous emission process. Several attempts to detect similar two-quantum decays in excited nuclei were not successful (108).

4. ATOMIC-BEAM TESTS OF SYMMETRY AND INVARIANCE PRINCIPLES

4.1 Intrinsic Electric Dipole Moments of the Neutron and Electron

4.1.1 Parity and time-reversal invariance: general considerations.

It is well known that the static electric dipole moment (EDM) of a physical system (atom, elementary particle) must be zero if the system is in a state of well-defined parity and if inversion symmetry (P) or time-reversal symmetry (T) hold (109). For, when (P) is considered first, the interaction of the intrinsic EDM (called $\underset{\sim}{\mu}$) with the electric field $\underset{\sim}{E}$ is of the form $\mathcal{H} = - \underset{\sim}{\mu} \cdot \underset{\sim}{E}$. Since $\underset{\sim}{E}$ is a polar vector ($P\underset{\sim}{E}P^{-1} = - \underset{\sim}{E}$), $\underset{\sim}{\mu}$ must be also, if P is to commute with H. However, if the state $|\psi\rangle$ has definite parity, then $P|\psi\rangle = \pm|\psi\rangle$, so that

$$\langle \psi | \underset{\sim}{\mu} | \psi \rangle = - \langle \psi | P \underset{\sim}{\mu} P | \psi \rangle = - \langle \psi | \underset{\sim}{\mu} | \psi \rangle .$$

Therefore $\langle \underset{\sim}{\mu} \rangle$ equals 0. Consider T next; suppose $|\psi\rangle$ is a state of well-defined angular momentum: $|\psi\rangle = |jm\rangle$. The operator T is anti-unitary and satisfies

$$T\underset{\sim}{J}T^{-1} = - \underset{\sim}{J}. \qquad 23.$$

Therefore:

$$TJ_z = - J_z T \qquad 24.$$

$$T(J_x \pm iJ_y) = - (J_x \mp iJ_y)T. \qquad 25.$$

From this we can easily show that

$$T|jm\rangle = (-1)^{j-m} e^{i\delta} |j, -m\rangle \qquad 26.$$

where δ is an unimportant phase factor. Now by a well-known theorem, we have

$$\langle jm | \underset{\sim}{\mu} | jm \rangle = C \langle jm | \underset{\sim}{J} | jm \rangle \qquad 27.$$

for all m, where C is a constant independent of m. However, if

$\mathcal{H}(= -\mu \cdot E)$ commutes with T, then since $TET^{\dagger} = +E$, we must also have

$$T\mu T^{\dagger} = +\mu \ . \qquad 28.$$

Thus

$$\begin{aligned} \langle jm | \mu | jm \rangle = \langle jm | T\mu T^{\dagger} | jm \rangle &= \langle j,-m | \mu | j,-m \rangle \\ &= C \langle j-m | J | j,-m \rangle \\ &= -\langle jm | \mu | jm \rangle \\ &= 0 \end{aligned} \qquad 29.$$

Experimental observations of small but finite $\langle \mu \rangle$ would therefore show breakdown of P and T.

4.1.2 Electric dipole moment of the free neutron. — A decade ago the first atomic-beam search for a neutron EDM was carried out by Smith, Purcell, and Ramsey (110). Essentially the same type of experiment is now being repeated in several laboratories (111) (Brookhaven, Oak Ridge), with numerous refinements and improvements to achieve a higher precision than that gained in the original work, in which the result

$$\mu_N < 2.4 \times 10^{-20} \text{ e.cm} \qquad 30.$$

was obtained. In the present Brookhaven experiment, a polarized beam of neutrons with intensity $\approx 10^6$ neutrons/min passes through a very strong electric field (≈ 50 kV/cm) located between two oscillating field regions separated by (L =) 90 cm. A homogeneous field of 1 gauss is maintained in the entire region, and neutron spin magnetic resonances occur at about 3 kHz with resonance linewidths of several hundred cycles per second. As described in Section 2, the presence of a finite EDM would be manifested by an electric-field-dependent phase shift of the neutron wave

function with respect to the applied rf. An improvement of several orders of magnitude is expected over the null result given in Equation 23.

4.1.3 Electric dipole moment of the electron. —No direct measurement of the electron EDM by any method similar to that employed for the free neutron would seem possible, because of the electron's charge. Earlier, various upper limits on the electron EDM were obtained from considerations of the Lamb shift (112), absence of parity-nonconserving atomic transitions in hydrogenic atoms (113), and also from scattering of high-energy electrons on ^{4}He (114). The most sensitive of these tests yielded $\mu_e < 1.2\times10^{-15}$ e. cm, which is a very crude result compared even with the old value for the neutron. For some time it did not appear possible to detect an electron's EDM from observation of an atom's EDM, since according to a theorem of Schiff (115), an electron's EDM would be completely neutralized by redistribution of atomic charge. However, Sandars (116) has shown that Schiff's argument is strictly valid only in the nonrelativistic limit. Sandars argued that the presence of an electronic EDM would add a term of the form

$$\mathcal{H}' = -\mu_e \sum_i \beta_i \underset{\sim}{\sigma}_i \cdot \underset{\sim}{E}_i \qquad 31.$$

to the unperturbed relativistic Hamiltonian:

$$\mathcal{H}^0 = \sum_i [\beta_i mc^2 + \underset{\sim}{\alpha}_i \cdot c\underset{\sim}{p}_i - eV_i] + \sum_{j\neq k} \frac{1}{2}\left[\frac{e^2}{r_{jk}} + B_{jk}\right] \qquad 32.$$

Here $\underset{\sim}{E}_i$ is the total electric field at the ith electron, μ_e is the free electron's EDM, B_{jk} is the Breit interaction, and β_i and $\underset{\sim}{\alpha}_i$ are the 4×4 Dirac matrices for the ith electron. Equation 31 can be rewritten:

$$\mathcal{H}' = \frac{\mu_e}{e}\left[\mathcal{H}^0, \sum_i \underset{\sim}{\sigma}_i \cdot \underset{\sim}{\nabla}_i\right] + \frac{\mu_e}{e}\left[\sum_i \underset{\sim}{\sigma}_i \cdot \underset{\sim}{\nabla}_i, \sum_{j\neq k} \frac{1}{2} B_{jk}\right]$$

$$+ \mu_e \sum_i (1-\beta_i)\underset{\sim}{\sigma}_i \cdot \underset{\sim}{E}_i \ . \qquad 33.$$

The expectation value of the first term is zero (Schiff's result), and that of the second can be shown to be quite small. Sandars has demonstrated that for the heavy alkalis the expectation value of the third term is appreciable, and that, in fact, the ratio of the cesiums' EDM to the electron's EDM is ≈ 100.

In several related experiments, Lipworth, Sandars, and coworkers (117, 118) searched for a cesium EDM by a method similar to that employed for the free neutron. They induced a resonance between the Cs ground-state Zeeman levels ($F=4$, $m_F=-3$) and ($F=4, m_F=-4$) in a weak magnetic field (see Figure 6, transition a) and adjusted the rf to the point of maximum slope on the central peak of the interference pattern of the separated oscillating fields. The beam passes between two condenser plates situated between the rf fields, and a voltage modulated at frequency ω is applied. The resulting signal at ω (linear Stark effect) is separated from the signal occuring at 2ω (due to quadratic Stark effect) with a phase-sensitive detector. The signal at ω could, of course, arise from spurious instrumental effects. For example, the atomic magnetic moment interacts with a magnetic field $\underline{v \times E}/c$ as it passes through the electric field. To guard against this, Sandars uses a symmetric beam machine with two ovens and two detectors, and with two beams going in opposite directions. At present the experimental results show that a cesium's EDM, if it exists, must be less than 10^{-20} e.cm. This implies, from Sandars' calculation, that the electron's EDM must be less than 10^{-22} e.cm. At the time of writing, work to refine these results continues.

4.2 Atomic Beams and Beta Decay

4.2.1 Coupling constants of beta decay. —Experiments in which the decay-in-flight of polarized neutron beams are observed have played an important role in the elucidation of the beta-decay coupling constants, and have contributed significantly to our understanding of beta decay (119). Recently my co-workers and I have observed the decay-in-flight of polarized beams of ^{19}Ne nuclei, to make a sensitive test of T invariance in the decay $^{19}\text{Ne} \rightarrow {}^{19}\text{F} + e^+ + \nu$ (120). In order to give a clear discussion of this work, let us briefly review the status of our knowledge of the coupling constants in beta decay, and also discuss the angular correlations occurring in allowed beta decay, which are utilized in the ^{19}Ne experiment.

Of the five primitive β decay interactions (S, V, T, A, and P), the scalar (S) and vector (V) are identified as Fermi type radiations, in which the total angular momentum carried off by the leptons in allowed decay is zero. The axial vector (A) and tensor (T) are Gamow-Teller type radiations, in which the lepton angular momentum for allowed decay is unity. Since the nucleons participating in β decay are nonrelativistic, the pseudo-scalar interaction P does not contribute. That the Fermi and Gamow-Teller radiations are solely V and A, respectively, is most convincingly demonstrated by the well-known results of angular correlation experiments with the decays of unpolarized ^{35}Ar (almost pure V), ^{23}Ne and ^{6}He (pure A), and ^{19}Ne and the free neutron (mixed V and A) (121, 122). The magnitude of the ratio of axial to vector coupling constants in nuclear β decay, $|C_A/C_V| = 1.18$, is obtained from the neutron ft value (123) and also from the average ft values of the $0^+ \rightarrow 0^+$ pure Fermi transitions of nuclei such as ^{14}O and ^{26}Al*. There remains the question of the relative phase ϕ of the coupling constants:

$$C_A/C_V = re^{i\phi} \quad . \tag{34.}$$

The quantity ϕ was determined in neutron decay (124), and the facts discussed above were verified by examination of the various angular correlations between the electron momentum $\underset{\sim}{p}$, anti-neutrino momentum $\underset{\sim}{q}$, and neutron spin polarization direction $\hat{I}$, all of which occur in the decay-in-flight of polarized neutrons. The results of these experiments can easily be understood by reference to the theoretical formula for the differential transition rate $d\lambda$ for an allowed beta decay for which $I_i = I_f = 1/2$. When summing over polarizations of the emitted electron, one finds (125):

$$d\lambda = \frac{F(\mp Z, E)p^2q^2dp\ d\Omega_e\ d\Omega_\nu}{2(2\pi)^5\hbar^7c} \cdot \xi\left\{1 + a\frac{\underset{\sim}{v}}{c}\cdot\hat{q} + \frac{\langle\underset{\sim}{I}\rangle}{I}\cdot\left[A\frac{\underset{\sim}{v}}{c} + B\hat{q} + D\left(\frac{\underset{\sim}{v}}{c}\times\hat{q}\right)\right]\right\}, \quad \text{(for } e^{\pm}\text{)} \tag{35.}$$

Here $F(\mp Z, E)$ is the Fermi function; $\underset{\sim}{p}$, $\underset{\sim}{v}$, and $\underset{\sim}{E}$ are the momentum, velocity, and energy, respectively, of the electron; $q = e^{-1}(E_{max}-E)$ is the magnitude of neutrino momentum, and $\hat{q}$ is a unit vector in its direction; and $d\Omega_e$ and $d\Omega_\nu$ are differential solid angles for electron and neutrino, respectively. The spin polarization of the initial nucleus is specified by $\langle\underset{\sim}{I}\rangle/I$. The quantities $\underset{\sim}{\xi}, \underset{\sim}{a}, \underset{\sim}{A}, \underset{\sim}{B}$, and $\underset{\sim}{D}$ are given by:

$$\xi = |C_V|^2|\langle 1\rangle|^2 + |C_A|^2|\langle\sigma\rangle|^2 \tag{36.}$$

$$a_\xi = |C_V|^2|\langle 1\rangle|^2 - \tfrac{1}{3}|C_A|^2|\langle\sigma\rangle|^2 \tag{37.}$$

$$A\xi = \pm\tfrac{2}{3}|C_A|^2|\langle\sigma\rangle|^2 - \sqrt{\tfrac{1}{3}}(C_VC_A^* + C_AC_V^*)\langle 1\rangle\langle\sigma\rangle \tag{38.}$$

$$B\xi = \mp\tfrac{2}{3}|C_A|^2|\langle\sigma\rangle|^2 - \sqrt{\tfrac{1}{3}}(C_VC_A^* + C_AC_V^*)\langle 1\rangle\langle\sigma\rangle \tag{39.}$$

$$D\xi = \frac{i}{\sqrt{3}}(C_VC_A^* - C_AC_V^*)\langle 1\rangle\langle\sigma\rangle \tag{40.}$$

where $\langle 1 \rangle$ and $\langle \sigma \rangle$ are the Fermi and Gamow-Teller matrix elements, respectively. In Formulae 37-40, corrections due to a final-state interaction between the electron and final nucleus are neglected. In this approximation $\underline{D}$ must be zero if time-reversal invariance (T) holds in beta decay, since $\underline{T}$ implies that C_A/C_V is real ($\phi = 0$ or 180 deg). Coulomb effects might contribute a finite amount to $\underline{D}$ even if $\underline{T}$ holds. However, to first order in $Z\alpha/p$, the Coulomb correction vanishes if scalar and tensor couplings are zero (125). (Here $\underline{Z}$ is the charge of the final nucleus.) Thus a precise measurement of $\underline{D}$ gives a sensitive test of $\underline{T}$.

The beta decay asymmetry coefficient $\underline{A}$ can be determined by observation of the fore-aft asymmetry in $e^{\pm}$ emission of polarized nuclei (126). No direct determination of the corresponding asymmetry coefficient $\underline{B}$ in neutrino emission can be made, but $\underline{B}$ can nevertheless be determined by observing coincidences of electrons and recoil ions emitted in the decay of polarized nuclei. One thereby infers the neutrino direction from conservation of momentum. The cross-correlation coefficient $\underline{D}$ can likewise be determined by observation of electron-recoil ion coincidences from decay of polarized nuclei.

Experiments to determine $\underline{A}$, $\underline{B}$, and $\underline{D}$ in neutron decay yielded the results:

$$\underline{A} = -0.11 \pm 0.02, \quad \underline{B} = +0.88 \pm 0.15, \quad \underline{D} = +0.04 \pm 0.05.$$

These results and the values $\langle \sigma \rangle = +\sqrt{3}$, $\langle 1 \rangle = +1$ for neutron decay, when inserted in Formulae 36 and 38-40, yield the values

$$|C_A/C_V| = 1.18 \qquad 41.$$

$$\phi = 175 \pm 6 \text{ deg.} \qquad 42.$$

consistent with $\underline{T}$ invariance.

The discovery of CP violation (127) in K_2 decay has generated wide interest in the question of possible T violation in weak interactions. There is no clear connection between the well-established CP violation in neutral K decay and a possible T violation in strangeness-conserving beta decay. Still, the issue is so fundamental that it is worthwhile to repeat the D experiment with a different beta transition. We chose ^{19}Ne for this study because of the relative ease of production of a polarized beam (18, 19), and because of its large decay matrix elements: $\langle 1 \rangle \cong 1$, $\langle \sigma \rangle = -1.46 \pm 0.08$. (Ref. 19).

The radioactivity is produced in the reaction $^{19}F(p,n)^{19}Ne$ at the Berkeley 88-inch cyclotron with a target containing SF_6 gas. The neon is separated from the SF_6 and delivered to an atomic beam source at 30°K from which it effuses in the $^1S_0$ ground state. The beam is made 25 times as intense by recirculating the radioactive gas through the source.

A conventional deflection magnet selects either of the nuclear polarization states $M_I = \pm 1/2$ (see Figure 13), and polarizations of approximately 0.80 are achieved, as confirmed by observation of the beam deflection pattern.

The beam path terminates in the asymmetry detector, a short cylinder with a long, narrow channel entrance and thin end walls with adjacent scintillation counters. The asymmetry detector monitors the beam intensity and polarization continuously. The ^{19}Ne atoms remain in the cylinder for about 2 sec, and make about 10^4 wall collisions. In spite of this, polarization is maintained parallel to the cylinder axis, and an asymmetry in positron emission by atoms decaying in the cylinder is observed, consistent with the value $A(^{19}Ne) = -0.033$ measured previously (18, 19).

To measure $D(^{19}Ne)$, the spin orientation of beam atoms in the coincidence detector chamber is maintained (as shown in Figure 13), with axial guiding coils. For measurements of $\underline{B}$, the polarization is kept perpendicular to the beam over the entire flight path from deflection magnet to asymmetry detector.

The coincidence chamber houses two detector banks, each containing four positron counters and four ion counters spaced alternately around an octagon. (See Figure 14.) The positron counters are conventional scintillators with discriminators set to accept pulses from positrons with kinetic energies greater than 0.7 MeV. (The maximum e^+ kinetic energy is 2.24 MeV.) The recoil ions $^{19}F^-$ possess kinetic energies in a continuous range up to 210 eV(121) compared with 0.003 eV for ^{19}Ne beam atoms). Recoil ions drift from the beam axis to the inner grid (Figure 14), are accelerated by an increment of 9 keV, and enter secondary emission detectors (128). The drift region enclosed by the inner grid is electric field-free. A weak magnetic field imposed to define the axis of polarization has negligible effect on the trajectories of the decay products. The symmetrical detector arrangement shown in Figure 14 has the advantage that many possible systematic errors that might otherwise be introduced into the data, cancel to high order.

The results of this investigation are:

$$B(^{19}Ne) = -0.90 \pm 0.13$$

$$D(^{19}Ne) = +0.002 \pm 0.014.$$

The latter implies that

$$\phi = 180.2 \pm 1.6 \text{ deg.}$$

again consistent with $\underline{T}$ invariance.

4.3 Experimental Limits for the Electron-Proton Charge Difference and for the Charge of the Neutron

Zorn, Chamberlain, and Hughes (129) have determined upper limits for the electric charges on the atoms of Cs and K and on the molecules H_2 and D_2 by molecular-beam-deflection in an intense electric field. The results can be interpreted as showing that the magnitude of the electron charge differs from that of the proton by less than 5 parts in 10^{19}, and that the neutron charge is less than 5×10^{-19} $|e|$. Still smaller upper limits ($\approx 4\times10^{-20}$) for the electron-proton charge difference are obtained in experiments by King (130), in which the change in potential of a metal container relative to its surroundings is observed as a gas (H_2, He) effuses from the container.

In addition to their general interest, these experiments are useful as a specific test of the suggestion made several years ago by Lyttleton and Bondi (131). They pointed out that if the electron-proton charge difference were only 2 parts in 10^{18} of the electron charge, the observed rate of expansion of the universe could be explained as an electric repulsion. Earlier, Einstein had pointed out that if the relative difference were only 3 parts in 10^{19}, one could understand the magnetic fields of the earth and sun as the fields of rotating charged bodies. The results of the recent experiments appear to rule out these suggestions.

5. STATIC PROPERTIES OF ATOMIC NUCLEI

5.1 The Isotope Shift

5.1.1 General method. — Marrus and collaborators (132, 133) have developed an ingenious atomic-beam method for investigating isotope shifts. They employ a conventional atomic-beam machine with flop-in geometry, the C region consisting of a pair of electric field plates capable of sustaining large electric fields. The space between the plates is illuminated by filtered resonance radiation from a commercial resonance lamp. In the work we describe, the $D_1(^2P_{1/2} - {}^2S_{1/2})$ transition in ^{133}Cs is employed. In the first experiments the radiation is a resolved doublet with peaks separated by the ground-state hfs splitting ($\approx$ 9000 MHz). (The hfs splitting of the $^2P_{1/2}$ state is small and can be ignored.)

Consider first the effect of the radiation on a beam of ^{133}Cs atoms. At zero electric field in the C region, beam-atom absorption lines coincide with the lamp emission lines, resonance absorption takes place, and in the ensuing decay, half of the atoms flip their spins and are thus refocused on the detector, giving a finite signal. When the electric field is turned on, the Stark effect depresses the energy levels of the $^2P_{3/2}$, $^2P_{1/2}$, and $^2S_{1/2}$ states and decreases the D_1 and D_2 separations (see Figure 16). The relative shifts of hfs levels and of Zeeman sublevels are negligibly small compared with the gross shifts of the levels themselves. If a sufficiently large electric field is applied to change the $^2P_{1/2}$- $^2S_{1/2}$ separation by more than the lamp linewidth, the beam detector signal goes to zero. If the electric field is increased enough more, the D_1 separation is reduced by an amount equal to the

$^2S_{1/2}$ hfs splitting. At this point the absorption lines and lamp emission lines overlap again, and another flop-in signal is observed. From the known ground-state hfs and assumed E^2 dependence of the Stark effect, the difference in $P_{1/2}$ and $S_{1/2}$ polarizabilities is determined in ^{133}Cs and ^{85}Rb. The results are in very good agreement with computed values (134, 135).

If one employs a ^{133}Cs absorption cell between the lamp and the beam, it becomes possible to narrow the absorption line considerably. The width of the cell absorption line is ordinarily determined by Doppler effect. However, if the atoms in the cell are in an atomic beam parallel to the main beam, the linewidth is more nearly the natural width. In this way the $^2P_{1/2}$ hfs is resolved and determined quantitatively. (See Figure 17).

5.1.2 Measurements of the isotope shift in Cs. — If one uses instead a beam of some other isotope (e.g., $^{134}Cs^m$), the lamp resonance line and the beam atom absorption line no longer match at zero electric field. However, application of the electric field decreases the D_1 separation in $^{134}Cs^m$ to a point where absorption can occur; in this way one obtains the isotope shift between ^{133}Cs and $^{134}Cs^m$ from knowledge of the Stark effect. At the time of writing, the additional isotopes of Cesium: A = 127, 129, 131, 134, and 137 – had been investigated relative to ^{133}Cs. All of the latter have zero isotope shift (± 15 mK). One would predict a finite volume shift of ≈ 11 mK/sec per neutron, and the results are therefore rather surprising.

5.2 Magnetic Moments of Mirror Nuclei

The magnetic moments of mirror nuclei are of interest, since

many of them can be predicted with reasonable accuracy from relatively simple nuclear models. If one knows the magnetic moments of both members of a mirror pair, it is useful to compare the moment sum with that predicted by theory, since in this sum, contributions to the individual moments arising from pionic exchange currents cancel (136). One hopes (vainly so far) to gain insight into the nature of these exchange current contributions.

The magnetic moments of the stable mirror nuclei were determined by conventional methods years ago. More recently the moments of many of their unstable partners have been measured with a variety of techniques. Although it is not an atomic-beam measurement, the recent work of Sugimoto et al. (137) on ^{17}F is worthy of special mention. In this experiment ^{17}F nuclei are produced in the $^{16}O(d,n)^{17}F$ reaction by deuteron bombardment of a thin foil of SiO_2. The recoil ^{17}F nuclei emitted at a definite angle possess considerable polarization. These nuclei are trapped on a surface of pure CaF_2 and remain there in the presence of a strong magnetic field, which defines an axis of quantization for nuclear magnetic resonance and decouples $\underline{I}$ and $\underline{J}$. The relaxation time for the nuclear spin polarization is comparable to the half life (66 sec), so that in β^+ decay, considerable anisotropy is observed in the fore-aft directions. When nuclear magnetic resonance is induced by an external coil, the anisotropy reverses.

In the work of Calaprice et al (138) on ^{35}Ar, similar to the ^{19}Ne work mentioned earlier (18, 19) ^{35}Ar atoms polarized in an atomic beam are stored in a thin-walled bulb, and the anisotropy of decays is observed with counters adjacent to the bulb walls. The anisotropy is

reversed when magnetic resonance is induced in a C field. From measurements of the anisotropy, one obtains a value of the axial vector reduced matrix element $\langle\sigma\rangle$ in the $^{35}Ar \rightarrow {}^{35}Cl$ decay; this value is considerably more precise than that derived from electron-neutrino angular correlation work (121).

Table IV lists the magnetic moments of mirror pairs of nuclei for which the moment is known for both members. The deviations of ^{3}H and ^{3}He moments from their respective "Schmidt" values are well accounted for by equal and opposite exchange current contributions, as is well known. One expects only small deviations from Schmidt values for the sum of moments of mirror nuclei which have an odd nucleon in the $P_{1/2}$ state (c.f. ^{13}N - ^{13}C and ^{15}D - ^{15}N) (151). In addition, very small deviations are expected for "doubly magic plus or minus one" nuclei (e.g., A = 15, A = 17). For A = 11, 19, 21, and 35, the situation is more complex. Here the deviations of individual moments from "single-particle model" values are in general large. Any accurate calculation of the moments should take into account the appreciable nuclear distortions and collective effects. For A = 11, this is particularly difficult since one must consider seven nucleons in the 1 p shell. The most extensive calculations have been done by Kurath (151). Here the predicted moments depend sensitively on the amount of spin-orbit coupling. If one chooses the coupling parameter to give the best agreement with low-lying excited-state energies, the experimental and theoretical moments disagree by about 0.5 nm.

For A = 19, a rotational model calculation (19) gives better agreement with the observed magnetic moment of ^{19}F and the low-lying

TABLE IV

Magnetic Moments of Mirror Nuclei

Parent					Daughter						
Nucleus	Half life		Magnetic moment Expt.	Theor.	Nucleus	Half life	Magnetic moment Expt.	Theor.	Magnetic moment Σ_1=expt	Σ_2=theor	$\Sigma_1-\Sigma_2$
n	11 min	1/2	-1.913[a]		p	1/2	2.793[j]		+0.880		
^{3}H	12 y	$1/2^+$	2.979[b]	2.793[s]	^{3}He	$1/2^+$	-2.127[k]	-1.913[s]	+0.852	+0.880	-0.028
^{11}C	21 min	$3/2^-$	(-)1.027[c]	-1.913[s]	^{11}B	$3/2^-$	+2.686[l]	+3.793[s]	1.659	1.880	-0.221
^{13}N	10 min	$1/2^-$	-0.321[d]	-0.264[s]	^{13}C	$1/2^-$	0.702[m]	0.638[s]	0.381	0.374	+0.007
^{15}O	123 sec	$1/2^-$	0.719[e]	+0.638[s]	^{15}N	$1/2^-$	-0.283[n]	-0.264[s]	0.436	0.374	+0.062
^{17}F	66 sec	$5/2^+$	4.722[f]	4.793[s]	^{17}O	$5/2^+$	-1.894[p]	-1.913[s]	2.828	2.880	-0.052
^{19}Ne	18 sec	$1/2^+$	-1.887[g]	-1.89 [g]	^{19}F	$1/2^+$	2.628[q]	2.74 [g]	0.741	0.85	-0.11
^{21}Na	23 sec	$3/2^+$	2.386[h]	2.41 [h]	^{21}Ne	$3/2^+$	-0.662[r]	-0.71 [h]	+1.724	+1.70	+0.024
^{35}Ar	1.8 sec	$3/2^-$	0.632[i]	0.48 [i]	^{35}Cl	$3/2^-$	+0.821[t]	+0.98 [i]	1.453	1.46	-0.01

[a] Reference 139

[b] Reference 140

[c] Reference 141

[d] Reference 17

[e] Reference 16

[f] Reference 137

[g] References 18, 19

[h] Reference 142

[i] Reference 138

[j] Reference 143

[k] Reference 144

[l] Reference 10

[m] Reference 145

[n] Reference 146

[p] Reference 147

[q] Reference 148

[r] Reference 149

[s] "Schmidt" value

[t] Reference 150.

excited-state energies of ^{19}Ne than previous calculations. A spin-orbit correction has the right sign and approximate magnitude to account for the remaining deviation in ^{19}F.

For $\underline{A}$ = 23, a collective model calculation gives rough qualitative agreement with the observed moments, and improves appreciably on the single-particle values. For $\underline{A}$ = 35, a rotational model calculation gives very close but almost certainly fortuitous agreement.

The remaining discrepancies cannot be accounted for in a quantitative and unambiguous way, owing to the obvious complexities of nuclear structure calculations. At present it seems quite hopeless to say anything definite about small pionic exchange current contributions to the magnetic moments of mirror nuclei.

It is a pleasure to thank my wife Ulla for her understanding and cooperation in the preparation of this article, and my colleagues H. M. Gibbs, R. Marrus, and E. H. Wichmann for numerous helpful suggestions and comments.

LITERATURE CITED

1. Ramsey, N. C., Molecular Beams (Clarendon Press, Oxford, 1956).
2. Kusch, P., and Hughes, V. W., Handbuch Der Physik 37 (Springer-Verlag, Berlin, 1959).
3. Kopfermann, H., Nuclear Moments (English version prepared from second German ed.)(Academic Press, New York, 1958).
4. Hubbs, J. C., and Nierenberg, W. A., Methods of Experimental Physics 5, Nuclear Physics, Part B, Yuan, L., and Wu., C. S., Editors (Academic Press, New York, 1963)
5. Ramsey, N. F., Ann. Rev. Nucl. Sci. 1, 97 (1951)
6. Pake, G. E., Ann. Rev. Nucl. Sci. 4, 33 (1954)
7. Nierenberg, W. A., Ann. Rev. Nucl. Sci. 7, 349 (1957)
8. Roberts, L. D., and Dabbs, J.W.T., Ann. Rev. Nucl. Sci. 11, 175 (1961)
9. Jeffries, C. D., Ann. Rev. Nucl. Sci. 14, 101 (1964)
10. Fuller, G. H., and Cohen, V. W., Nuclear Moments, Appendix I to Nuclear Data Sheets (USAEC, May 1965)
11. Perl, M. L., Rabi, I. I., and Senitzky, B., Phys. Rev. 97, 838; and 98, 611 (1955)
12. Weinreich, G., and Hughes, V., Phys. Rev. 95, 1451 (1954); Drake, C., Hughes, V., Lurio, A., and White, J., Phys. Rev. 112, 1627 (1958)
13. Faust, W., Lichten, W., and McDermott, M., Phys. Rev. 120, 469 (1960)
14. Robiscoe, R. T., Phys. Rev. 138, A22 (1965)
15. Goldenburg, H. M., Keppner, D., and Ramsey, N. F., Phys. Rev. Letters 5, 361 (1960)

16. Commins, E. D., and Feldman, H. R., Phys. Rev. 131, 700 (1963).

17. Bernstein, A. M., et al., Phys. Rev. 136, B27 (1964)

18. Commins, E. D., and Dobson, D. A., Phys. Rev. Letters 10, 347 (1963).

19. Dobson, D. A., Lawrence Radiation Laboratory Report, UCRL-11169 (1963)

20. See Reference 2, Sec. 13, pg. 28

21. Lew, H., Phys. Rev. 76, 1086 (1949)

22. Hobson, J. P., Hubbs, J. C., Nierenberg, W. A., Silsbee, H. B., and Sunderland, R. J., Phys. Rev. 104, 101 (1956).

23. Lamb, W. E., and Retherford, R. C., Phys. Rev. 79, 549 (1950)

24. Hagstrum, H., Phys. Rev. 96, 325, 336 (1954); 104, 672 (1956)

25. Lemonick, A., Pipkin, F., and Hamilton, D., Rev. Sci. Instr. 26, 1112 (1955)

26. Rabi, I. I., Ramsey, N. F., and Schwinger, J., Rev. Mod. Phys. 26, 167 (1954)

27. Bloch, F., and Siegert, A. J., Phys. Rev. 57, 522 (1940). See also Ramsey, N. F., Phys. Rev. 100, 1191 (1955)

28. Majorana, E., Nuovo Cimento 9, 43 (1932)

29. Ramsey, N. F., Phys. Rev. 78, 695 (1950)

30. Ramsey, N. F., and Silsbee, H. B., Phys. Rev. 84, 506 (1951).

31. Torrey, H. C., Phys. Rev. 59, 293 (1941); see also Salwen, H., Phys. Rev. 101, 621 (1956)

32. See, for example: Jaccarino, V., King, J. G., Satten, R. A., and Stroke, H. H., Phys. Rev. 94, 1798 (1954); see also Brown, H. H., and King, J. G., Phys. Rev. 142, 53 (1966)

33. Fermi, E., Z. Physik 60, 320 (1930)

34. See Reference 1, pages 74 and 75

35. See Reference 2, sec. 35, pg. 84

36. See Reference 3, pg. 123

37. Rosenthal, J. E., and Breit, G., Phys. Rev. 41, 459 (1932)

38. Bohr, A., and Weisskopf, V. F., Phys. Rev. 77, 94 (1950).

39. Schwartz, C., Phys. Rev. 99, 1035 (1955)

40. Sternheimer, R., Phys. Rev. 80, 102 (1950); 84, 244 (1951); 86, 316 (1952); 95, 736 (1954)

41. Breit, G., and Rabi, I. I., Phys. Rev. 38, 2082 (1931)

42. See Reference 1, Appendix C, Equations C.24, C.26, C.27

43. See Reference 2, Equation 34, 12

44. Karplus, R., and Klein, A., Phys. Rev. 87, 848 (1952)

45. Weinstein, R., Deutsch, M., and Brown, S. C., Phys. Rev. 94, 758 (1954); and 98, 233 (1955)

46. Hughes, V. W., Marder, S., and Wu, C. S., Phys. Rev. 106, 934 (1957)

47. Hughes, V. W., Ann Rev. Nucl. Sci. 16, 445 (1966)

48. Cleland, W. E., et al., Phys. Rev. Letters 13, 202 (1964)

49. Thomson, P., et al., Bull. Am. Phys. Soc. 12, 75, (1967)

50. Crampton, S. B., Kleppner, D., and Ramsey, N. F., Phys. Rev. Letters 11, 338 (1963)

51. Heberle, J. W., Reich, H., and Kusch, P., Phys. Rev. 101, 612 (1956)

52. Crampton, S. B., et al., Phys. Rev. 141, 55 (1966)

53. Reich, H. A., Heberle, J. W., and Kusch, P., Phys. Rev. 104, 1585 (1956)

54. Prodell, A. G., and Kusch, P., Phys. Rev. 106, 87 (1957)

55. Fortson, E. N., Major, F. G., and Dehmelt, H. G., Phys. Rev. Letters 16, 221 (1966)

56. Novick, R., and Commins, E. D., Phys. Rev. 111, 822 (1958)

57. Hutchinson, D. P., Menes, J. Shapiro, G., and Patlach, A. M., Phys. Rev. 131, 1351 (1963)

58. Ruderman, M. A., Phys. Rev. Letters 17, 794 (1966)

59. Kleppner, D., Goldenberg, H. M., and Ramsey, N. F., Appl. Opt. 1, 55 (1962)

60. Kleppner, D., Goldenberg, H. M., and Ramsey, N. F., Phys. Rev. 126, 603 (1962)

61. Berg, H. C., and Kleppner, D., Rev. Sci. Instr. 33, 248 (1962)

62. Kusch, P., Phys. Rev. 100, 1188 (1955)

63. Wittke, J. P., and Dicke, R. H., Phys. Rev. 103, 620 (1956)

64. Pipkin, F. M., and Lambert, R. H., Phys. Rev. 127, 787 (1962)

65. Myint, T., Kleppner, D., Ramsey, N. F., and Robinson, H. G., Phys. Rev. Letters 17, 405 (1966)

66. Wilkinson, D. T., and Crane, H. R., Phys. Rev. 130, 852 (1963)

67. Breit, G., and Meyerott, R. E., Phys. Rev. 72, 1023 (1947)

68. Breit, G., Phys. Rev. 35, 1447 (1930)

69. Kroll, N., and Pollack, F., Phys. Rev. 86, 876 (1952)

70. Zwanziger, D. E., Bull. Am. Phys. Soc. 6, 514 (1961)

71. Layzer, A. J., ibid., 6, 514 (1961)

72. Newcomb, W. A., and Salpeter, E., Phys. Rev. 97, 1146 (1955)

73. Arnowitt, R., Phys. Rev. 92, 1002 (1953)

74. Iddings, C., Phys. Rev. 138, B446 (1965)

75. Zwanziger, D., private communication

76. Cohen, E. R., and DuMond, J. W. M., Rev. Mod. Phys. 37, 537 (1965)

77. Bohr, A., Phys. Rev. 73, 1109 (1948)

78. Greenberg, D., and Foley, H., Phys. Rev. 120, 1684 (1960)

79. Adams, E. N., II, Phys. Rev. 81, 1 (1951)

80. Dehmelt, H. G., and Major, F. G., Phys. Rev. Letters 8, 213 (1962)

81. Dehmelt, H. G., private communication

82. Zwanziger, D., Phys. Rev. 121, 1128 (1961)

83. Sternheim, M. M., Phys. Rev. 130, 211 (1963)

84. Goldwire, Jr., H. C., Phys. Rev. Letters 18, 433 (1967)

85. Lamb, Jr., W. E., and Retherford, R. C., Phys. Rev. 79, 549 (1950); and Phys. Rev. 81, 222 (1951)

86. Lamb, Jr., W. E., Phys. Rev. 85, 259 (1952)

87. Lamb, Jr., W. E., and Retherford, R. C., Phys. Rev. 86, 1014 (1952)

88. Triebwasser, S., Dayhoff, E., and Lamb, Jr., W. E., Phys. Rev. 89, 98 (1953)

89. Dayhoff, E., Triebwasser, S., and Lamb, Jr., W. E., Phys. Rev. 89, 106 (1953)

90. Lipworth, E., and Novick, R., Phys. Rev. 108, 1434 (1957)

91. Robiscoe, R. T., Phys. Rev. 138, A22 (1965)

92. Robiscoe, R. T., and Cozens, B. L., Phys. Rev. Letters 17, 69 (1966)

93. Robiscoe, R. T., and Cozens, B. L., Bull. Am. Phys. Soc. 11, 62 (1966)

94. Soto, Jr., M. F., Phys. Rev. Letters 17, 1153 (1966)

95. Kleinpoppen, H., Z. Physik 164, 174 (1961)

96. Wilcox, L. R., Lamb, Jr., W. E., and Sandars, T. M., Phys. Rev. 119, 1901 (1960); and Wilcox, L. R., and Lamb, Jr., W. E., Phys. Rev. 119, 1915 (1960)

97. Harriman, J. M., Phys. Rev. 101, 594 (1956)

98. Leventhal, M., Lea, K. R., and Lamb, Jr., W. E., Phys. Rev. Letters 15, 1013 (1965)

99. Lea, K. R., Leventhal, M., and Lamb, Jr., W. E., Phys. Rev. Letters 16, 163 (1966)

100. Fan, C. Y., Garcia-Munoz, M., and Sellin, I. A., Phys. Rev. Letters 15, 15 (1965)

101. Parker, W. H., Taylor, B. N., and Langenberg, D. N., Phys. Rev. Letters 18, 287 (1967)

102. Schwartz, C., Phys. Rev. 134, A1181 (1964)

103. Pichanick, F., Swift, R., and Hughes, V. W., Bull. Am. Phys. Soc. 9, 90 (1964)

104. Lipeles, M. Novick, R., and Tolk, N., Phys. Rev. Letters 15, 690 (1965)

105. Breit, G., and Teller, E., Astrophys. J. 91, 238 (1940)

106. Spitzer, L., and Greenstein, J., Astrophys. J., 114, 407 (1951)

107. Shapiro, J., and Breit, G., Phys. Rev. 113, 179 (1959)

108. Alburger, D. F., and Parker, P. D., Phys. Rev. 135, B294 (1964)

109. Landau, L., Nucl. Phys. 3, 127 (1957)

110. Smith, J. H., Purcell, E. M., and Ramsey, N. F., Phys. Rev. 108, 120 (1957)

111. Cohen, V. W., private communication

112. Feinberg, G., Phys. Rev. 112, 1637 (1958)

113. Salpeter, E. E., Phys. Rev. 112, 1642 (1958)

114. Goldemberg, J., and Torizuka, Y., Phys. Rev. 129, 2580 (1963)

115. Schiff, L. I., Phys. Rev. 132, 2194 (1963)

116. Sandars, P. G. H., Phys. Letters 14, 194 (1965)

117. Sandars, P. G. H., and Lipworth, E., Phys. Rev. Letters 13, 718 (1964)

118. Carrico, J., Thesis, Brandeis University, Waltham, Mass., 1966

119. For excellent reviews of beta decay see: Konopinski, E. J., Ann. Rev. Nucl. Sci. 9, 99 (1959); Konopinski, E. J., The Theory of Beta Radioactivity, (Clarendon Press, Oxford, 1966); Wu, C. S., and Moszkowski, S. A., Beta Decay (Interscience, New York, 1966)

120. Calaprice, F. P., Commins, E. D., Gibbs, H. M., Wick, G. L., and Dobson, D. A. (to be submitted to Phys. Rev. Letters)

121. Allen, J. S., et al., Phys. Rev. 116, 134 (1959)

122. Trebukhovski, A., et al., Soviet Physics (JETP) 36, 931 (1959)

123. Sosnovsky, A. N., et al., Nucl. Phys. 10, 395 (1959)

124. Burgy, M. T., et al., Phys. Rev. 120, 1827 (1960)

125. Jackson, J. D., Treiman, S. B., and Wyld, H. W., Nucl. Phys. 4, 206 (1957)

126. The first observations of this kind, on ^{60}Co, were reported by Ambler, E., et al., Phys. Rev. 106, 1361 (1957); 108, 503 (1957); and 110, 787 (1957)

127. Christenson, J. H., et al., Phys. Rev. Letters 13, 138 (1964)

128. Gibbs, H. M., and Commins, E. D., Rev. Sci. Instr. 37, 1385 (1966)

129. Zorn, J., Chamberlain, G., and Hughes, V. W., Phys. Rev. 129, 2566 (1963)

130. King, J. G., Phys. Rev. Letters 5, 562 (1960)

131. Lyttleton, R. A., and Bondi, H., Proc. Roy. Soc. (London), A252 , 313 (1959)

132. Marrus, R., and McColm, D., Phys. Rev. Letters 15, 813 (1965)

133. Marrus, R., McColm, D., and Yellin, J., Phys. Rev. 147, 55 (1966)

134. Stone, P. M., Phys. Rev. 127 , 1151 (1962)

135. Bates, D. R., and Damgaard, A., Phil. Trans. Roy. Soc. (London), A242, 101 (1949)

136. Sachs, R. G., Nuclear Theory (Addison Wesley, Cambridge, Mass., 1954), Chapt. 9

137. Sugimoto, K., Mizobuchi, A., Nakai, K., and Matuda, K., Phys. Letters 18, 38 (1965)

138. Calaprice, F. P., Commins, E. D., and Dobson, D., Phys. Rev. 137, B1453 (1965)

139. Cohen V. W., Corngold, N. R., and Ramsey, N. F., Phys. Rev. 104, 283 (1956)

140. Duffy, W., Phys. Rev. 115, 1012 (1959)

141. Haberstroh, R. A., et al., Phys. Rev. 136, B932 (1964)

142. Ames, O., Phillips, E. A., and Glickstein, S. S., Phys. Rev. 137, B1157 (1965)

143. Vigoreaux, P., Nature 198, 1188 (1963)

144. Anderson, H. L., Phys. Rev. 76, 1460 (1949)

145. Royden, V., Phys. Rev. 96, 543 (1954)

146. Baldeschweiler, J. D., J. Chem. Phys. 36, 152 (1962)

147. Adler, F., and Yu, F. C., Phys. Rev. 81, 1067 (1951)

148. Baker, M. R., Anderson, C. H., and Ramsey, N. F., Phys. Rev. 133, A1533 (1964)

149. La Tourette, J. T., Quinn, W. E., and Ramsey, N. F., Phys. Rev. 107, 1202 (1957)

150. Ting, Y., and Williams, D., Phys. Rev. 89, 595 (1953)

151. Kurath, D., Phys. Rev. 124, 552 (1961)

CAPTIONS FOR ILLUSTRATIONS

Fig. 1. Schematic diagram of standard atomic-beam magnetic resonance apparatus of flop-in type, including (1) collimator slit, (2) rf transition region, and (3) beam stop. Atoms in beams a undergo rf resonance reorientation in (2) and are refocused on detector. Beams b are deflected out. Beam deflections are grossly exaggerated for pictorial clarity.

Fig. 2. Cross section of typical two-wire deflection magnet. For magnetization well below saturation values, the pole tip surfaces α and β coincide with magnetic equipotentials which would be produced by two equal and opposite line currents (1) and (2) perpendicular to page. At point, P, the field is in the z direction with $\partial B/\partial z = 0.98\, B/a$. The field gradient varies by only a small amount from this over beam height (the beam cross section indicated by dotted lines).

Fig. 3. Cross section of pole-tip arrangement for "hexapole" deflecting field. To a good approximation the force on a magnetic dipole moment in this field varies as μr, independent of θ.

Fig. 4. Typical resonance curve of Ramsey separated oscillating fields for a beam with Maxwellian velocity distribution. The central fringe is a maximum for zero relative phase of the two separated rf fields. The width of the central fringe is $\approx v/L$, and that of the envelope is $\approx v/\ell$.

Fig. 5. Breit-Rabi diagram for $I = 1/2$, $J = 1/2$, $\mu_I > 0$ (e.g., the $1^2S_{1/2}$ state of hydrogen or muonium). The states are labeled by m_F, but m_F is a good quantum number only for $x = 0$.

Fig. 6. Breit-Rabi diagram for $I = 7/2$, $J = 1/2$, $\mu_I > 0$ (e.g., the $6^2S_{1/2}$ ground state of ^{133}Cs). Various transitions of interest (a-e) are described in text.

Fig. 7. Schematic diagram of the atomic hydrogen maser. (See also Reference 50.)

Fig. 8. Ion trap and optically pumped Cs beam apparatus for the study of He^+ rf spectra. The quadrupole electrode surfaces are hyperboloids of revolution. Ion trapping times of about 20 minutes have been achieved. From Dehmelt and Major (Reference 80; see also Reference 55).

Fig. 9. Zeeman effect of the n=2 fine-structure levels of hydrogen or singly ionized helium. Hyperfine structure is neglected.

Fig. 10. Schematic diagram of level-crossing apparatus for the study of the Lamb shift in H and D, n=2. (see Robiscoe, References 91, 92, and 93).

Fig. 11. Zeeman effect of the n=2, J = 1/2 states of hydrogen including hfs. Of the 4 β-e level crossings, two (A, B) have been measured by Robiscoe (91, 92, 93).

Fig. 12. Observation of quenching of the metastable state β_B near the β_B-e_B crossing point. The experimental points (o) are compared with a line shape derived from the Bethe-Lamb theory of the lifetime of the 2S state in external fields. From Robiscoe (91).

Fig. 13. Schematic diagram of ^{19}Ne atomic-beam apparatus for investigation of time-reversal invariance in beta decay. (A) Asymmetry detector; (C_{1-3}) Differential pumping chambers; (D_{1-2}) Detector banks. Spin and magnetic field orientations are shown for D experiment. Beam deflections are grossly

exaggerated for clarity as in Fig. 1. The separation of the $M_I = \pm 1/2$ beams in the detector chamber is actually less than 0.05 cm.

Fig. 14. Schematic diagram of one detector bank, ^{19}Ne experiment. Ion detectors are labeled 1-4 and positron detectors are labeled a-d. The beam is directed into the page. For B experiment, in which coincidence pairs a-2, b-4 are compared with pairs d-2, c-4, respectively, spin orientation is along x axis. For D experiment, ^{19}Ne spin is into or out of page; coincidence pairs a-2, b-1, c-4, and d-3 are compared to pairs a-1, b-4, c-3, and d-2, respectively. A typical a-2 event is shown, with $\hat{p}$, $\hat{q}$, and $\hat{r}$ in directions of positron, neutrino, and recoil ion, respectively.

Fig. 15. Positron-^{19}F-recoil-ion coincidence counts versus delay time. Delayed coincidences occuring in the time interval 1.75-3.25 μsec are used in B and D measurements. The curve is obtained from a calculation of the geometry and the theoretical ion energy distribution, with a correction for beam scattering by residual gas. The points are experimental.

Fig. 16. The D_1 energy levels and transitions in ^{133}Cs, with the hfs of the $6^2P_{1/2}$ state neglected.

Fig. 17. The D_1 energy levels and transitions in ^{133}Cs with the hfs of the $6^2P_{1/2}$ state resolved. Signal $\underline{\alpha}$ occurs at zero electric field. Signals $\underline{\beta}$, $\underline{\gamma}$, and $\underline{\delta}$ occur at successively higher electric fields.

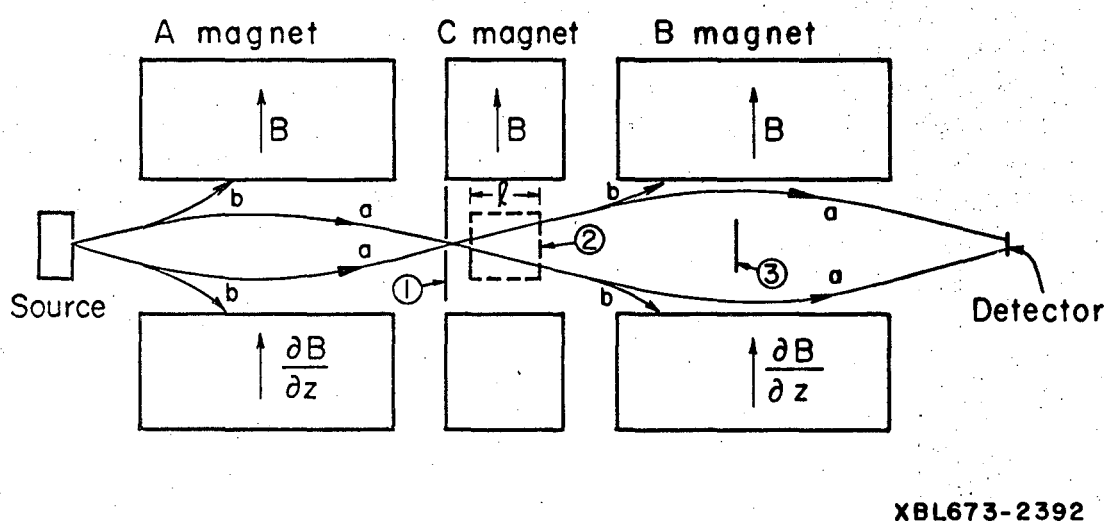
A magnet
C magnet
B magnet
B
B
B
l
b
a
a
b
a
b
a
b
Source
Detector
1
2
3
∂B/∂z
∂B/∂z
XBL673-2392

Fig. 1

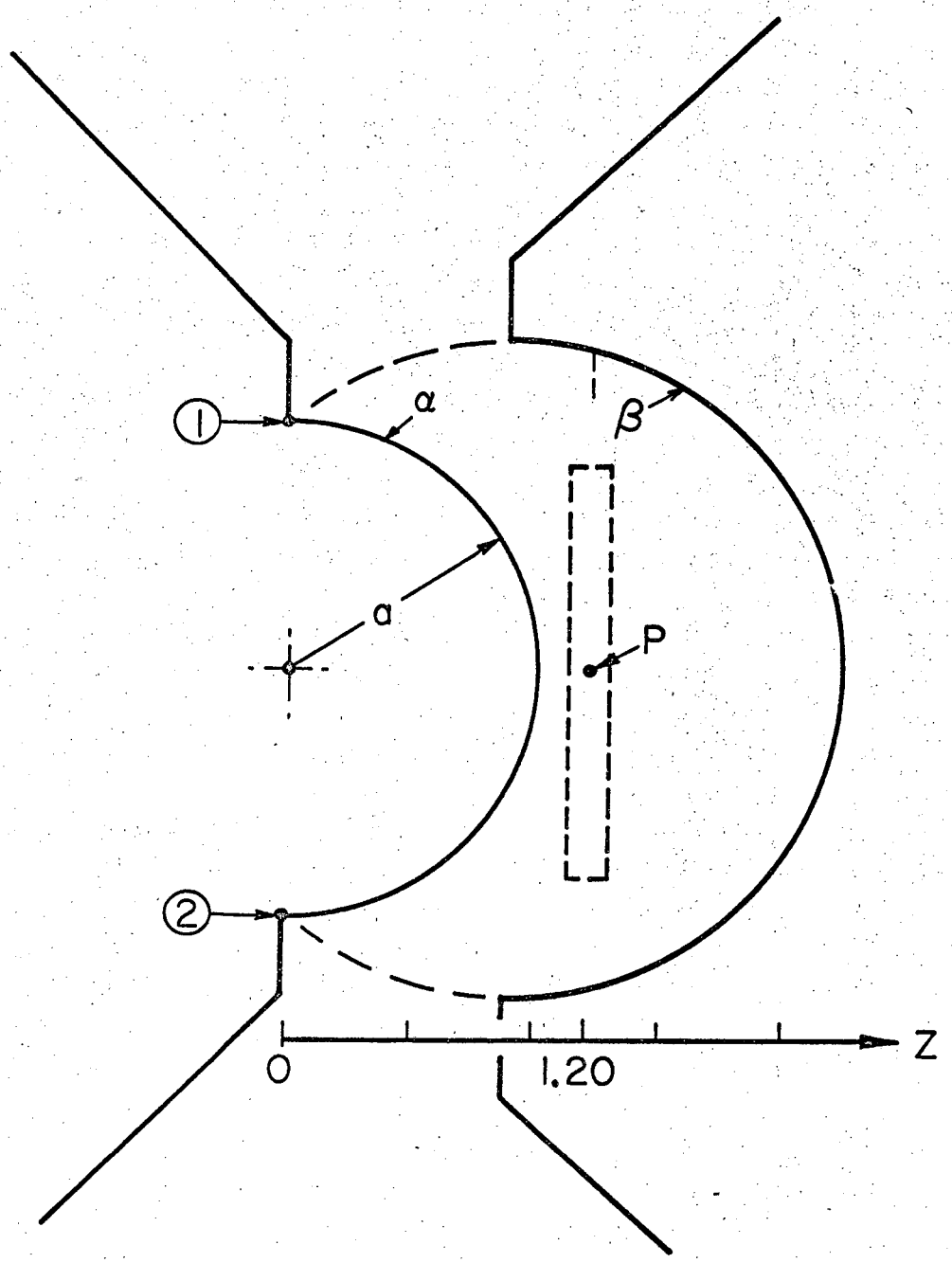

Fig. 2 XBL673-2393

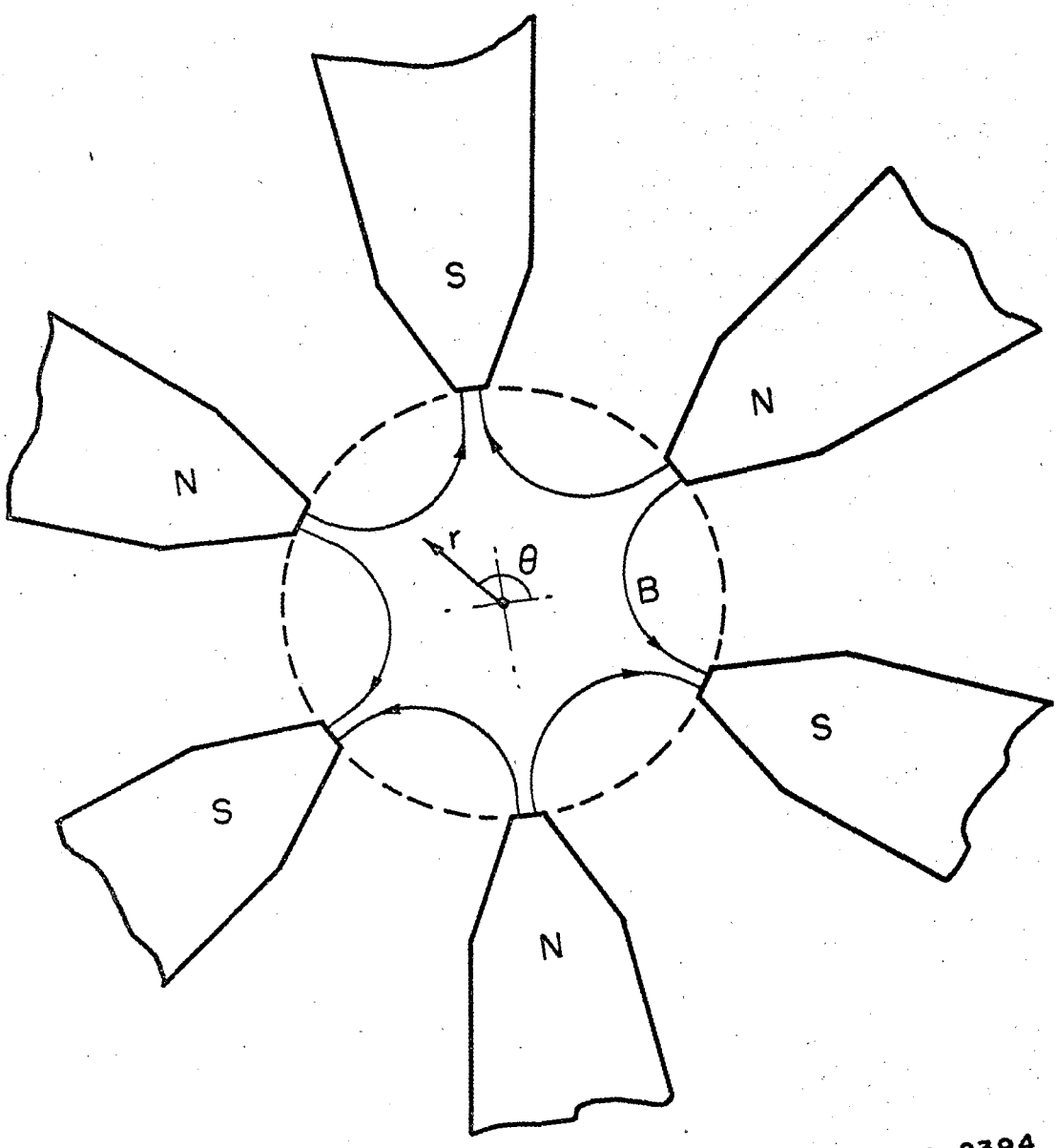

Fig. 3 XBL673-2394

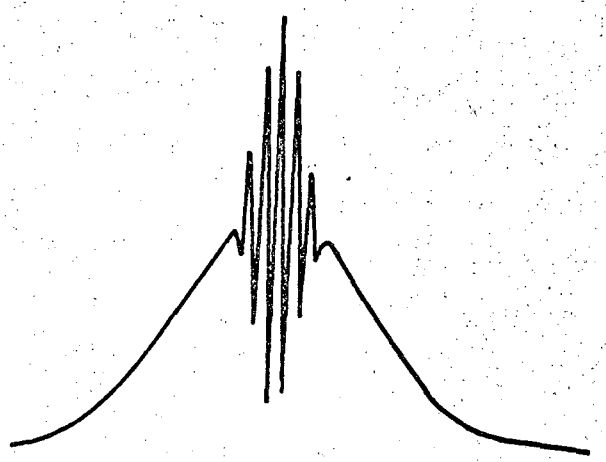

XBL673-2407

Fig. 4

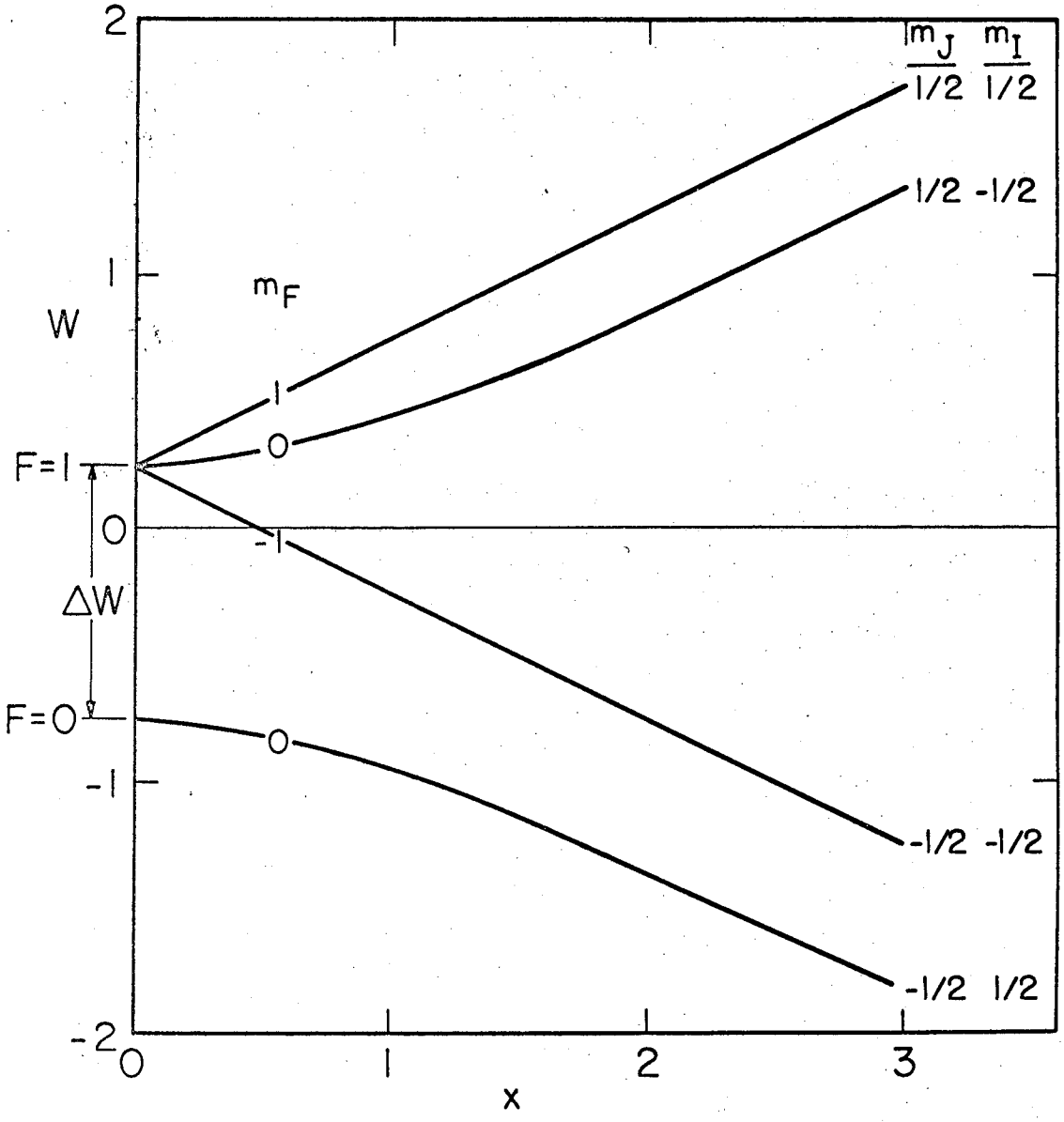

Fig. 5

XBL673-2395

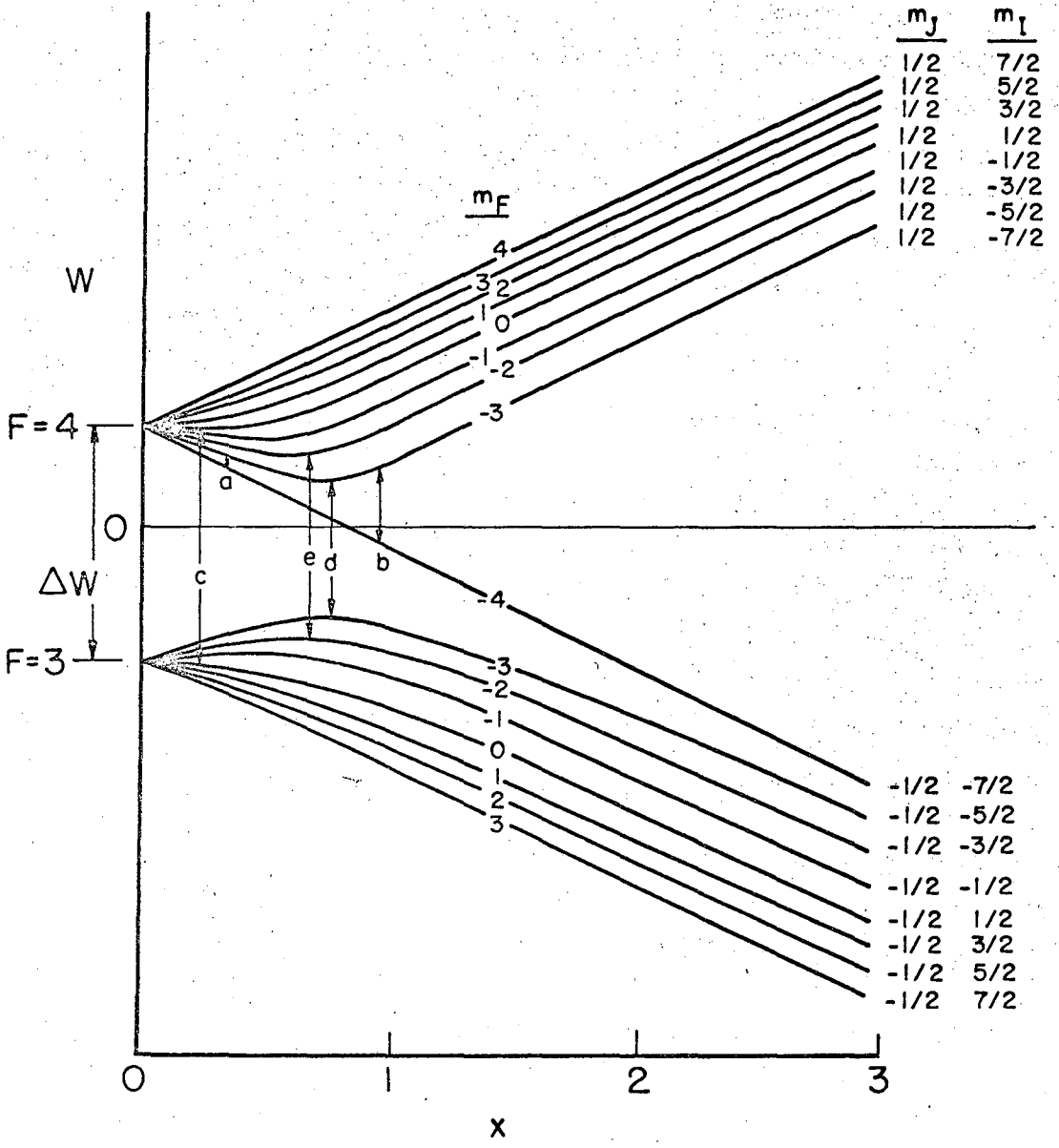

Fig. 6 XBL673-2396

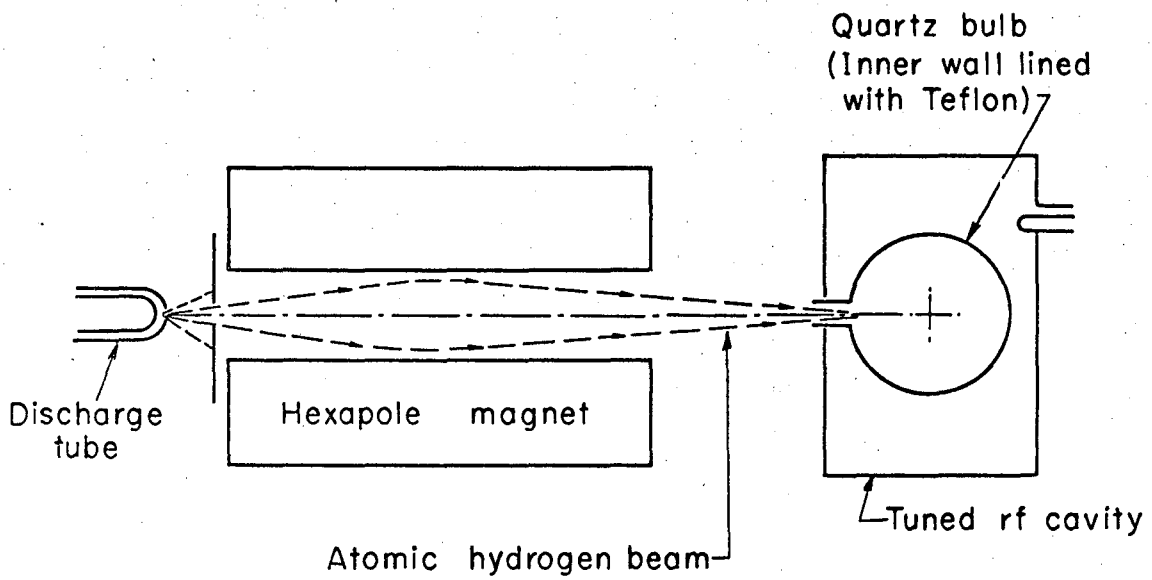

XBL673-2456

Fig. 7

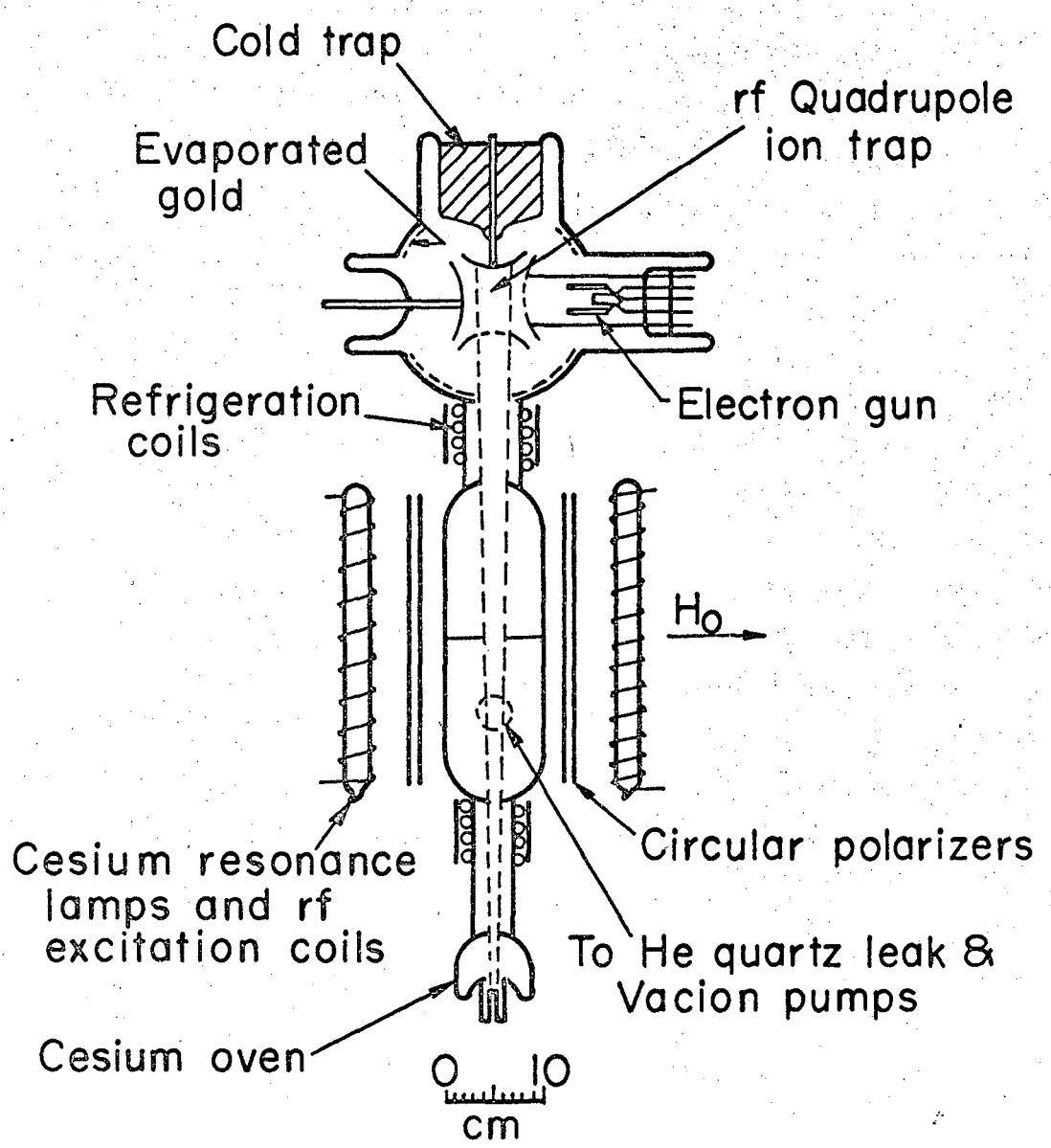

XBL673-2397

Fig. 8

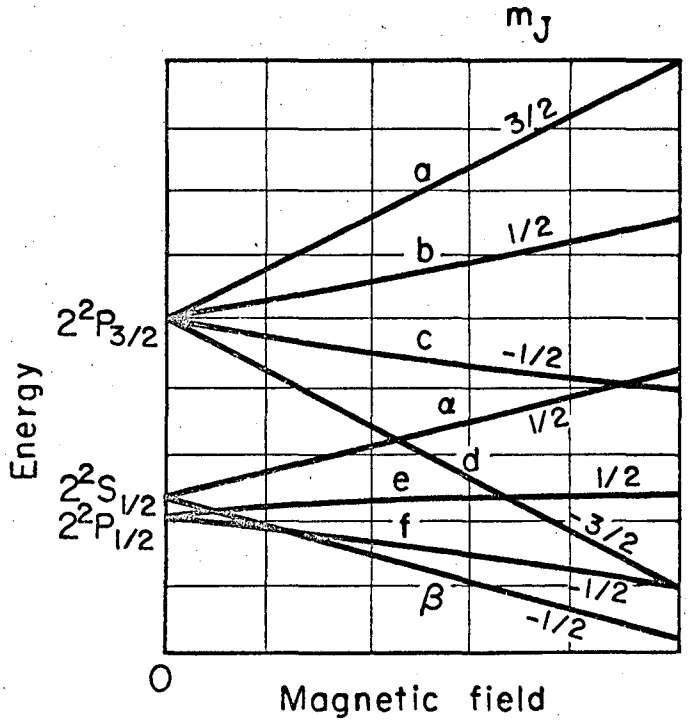

XBL673-2398

Fig. 9

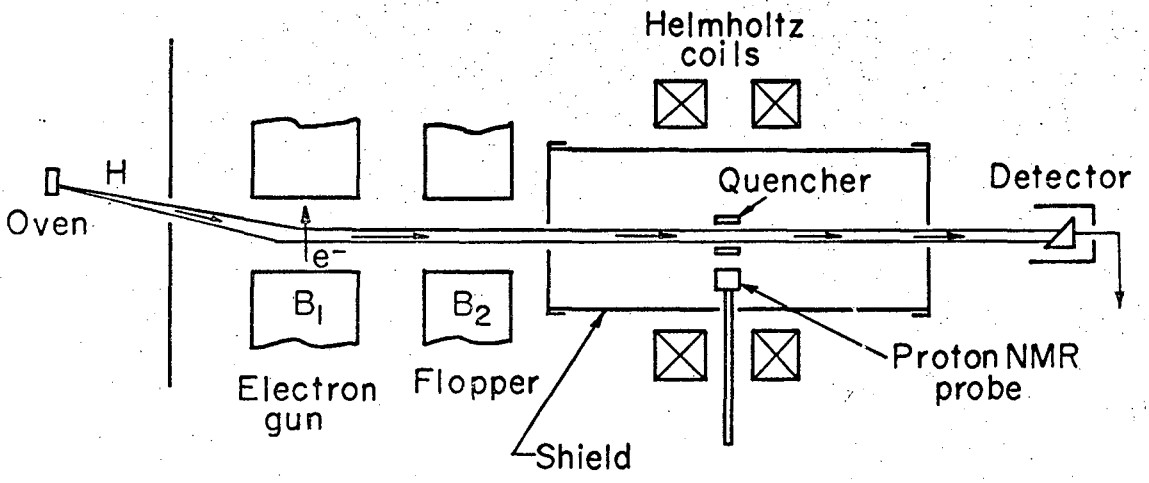

XBL673-2399

Fig. 10

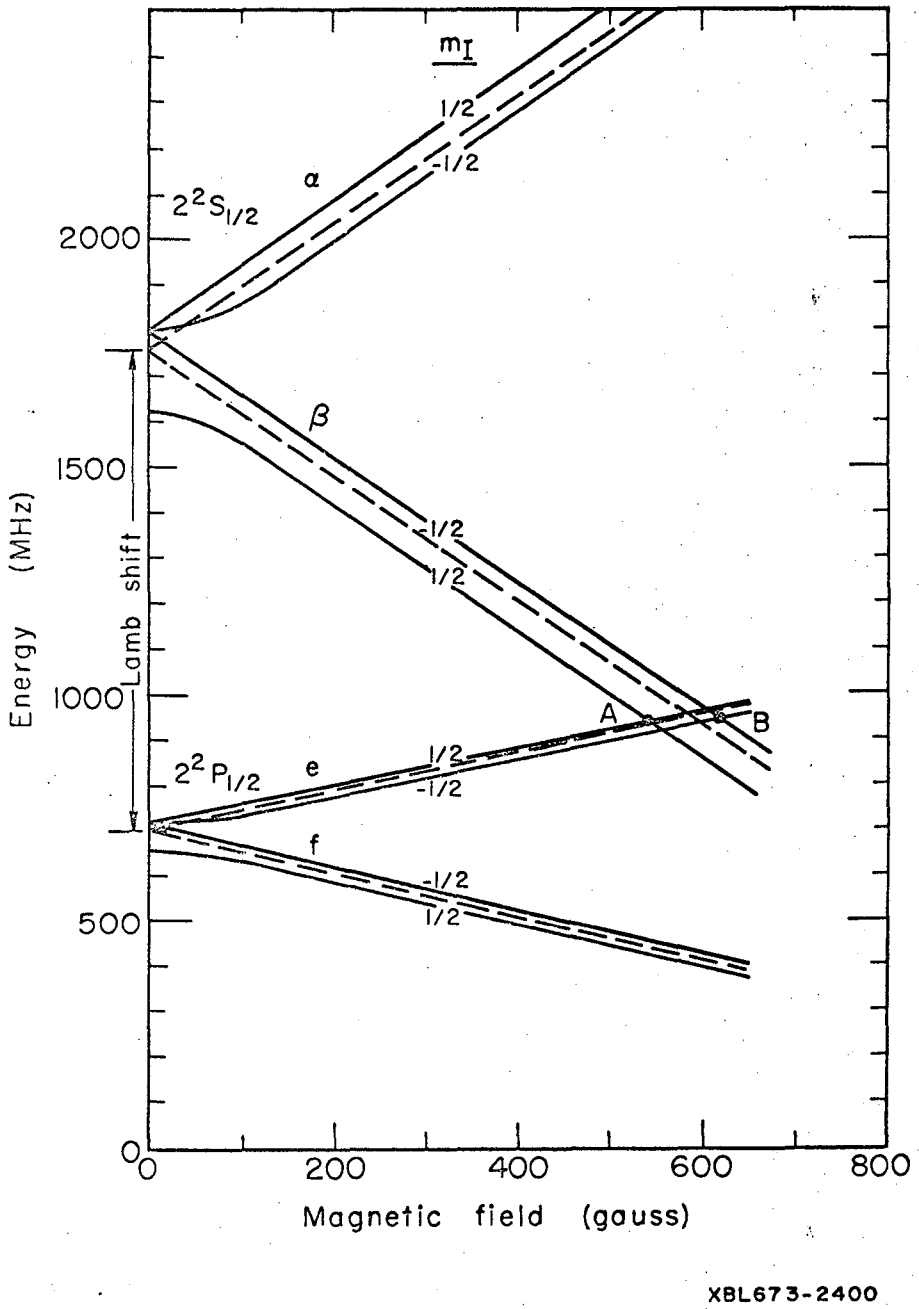
m_I
1/2
-1/2
α
$2^2S_{1/2}$
2000
β
1500
-1/2
1/2
Energy (MHz)
Lamb shift
1000
A
B
$2^2P_{1/2}$
e
1/2
-1/2
f
-1/2
1/2
500
0
0
200
400
600
800
Magnetic field (gauss)
XBL673-2400

Fig. 11

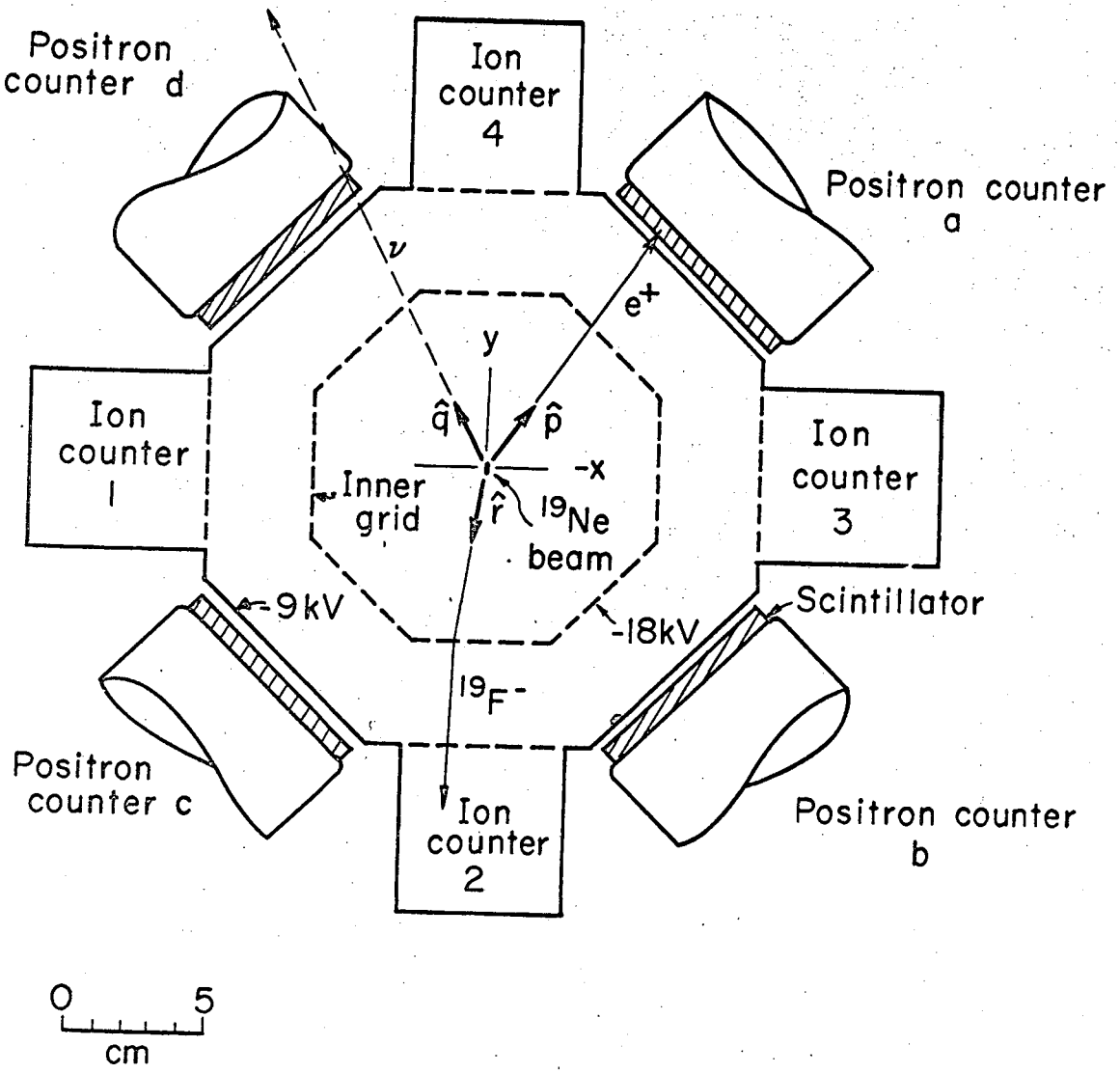

Fig. 14 XBL673-2403

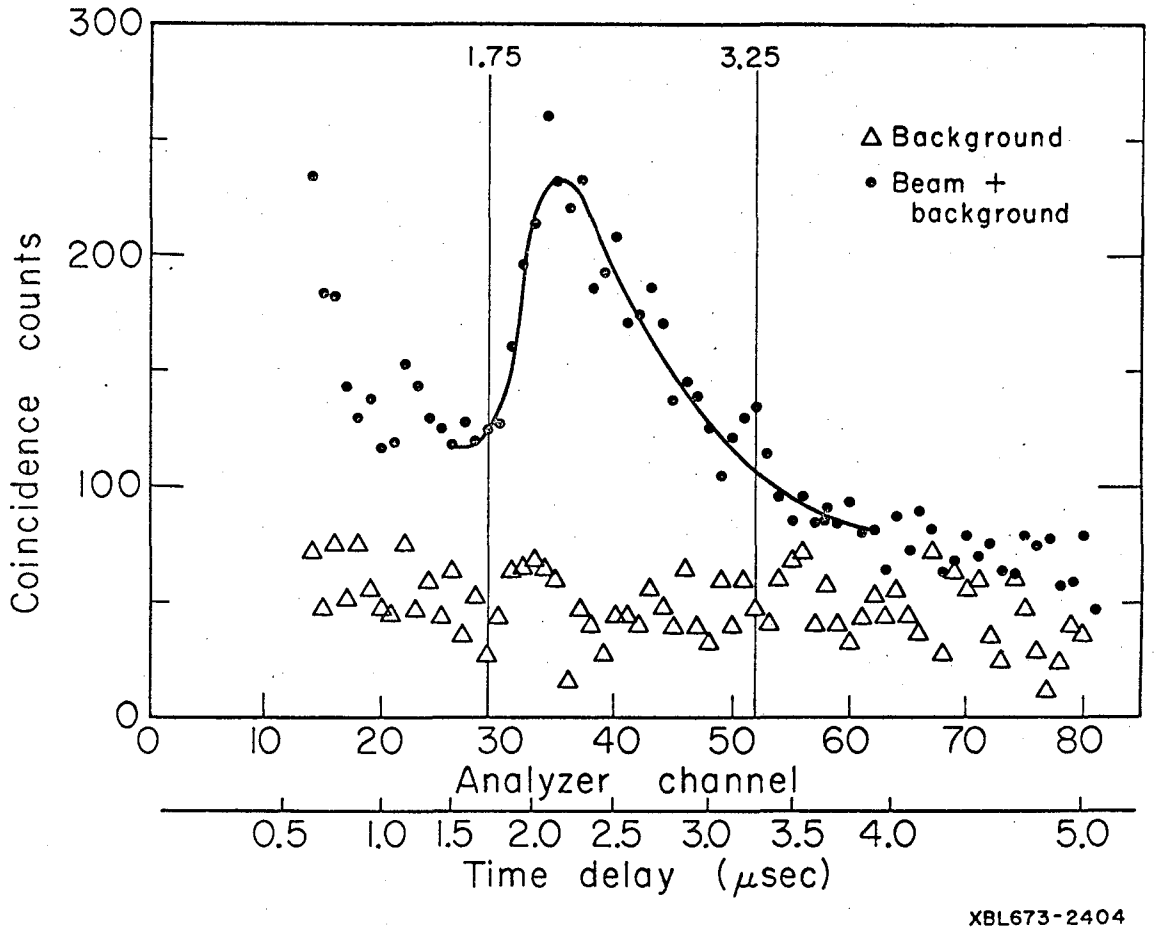
300
200
100
0
Coincidence counts
1.75
3.25
Background
Beam + background
0
10
20
30
40
50
60
70
80
Analyzer channel
0.5
1.0
1.5
2.0
2.5
3.0
3.5
4.0
5.0
Time delay (μsec)
XBL673-2404

Fig. 15

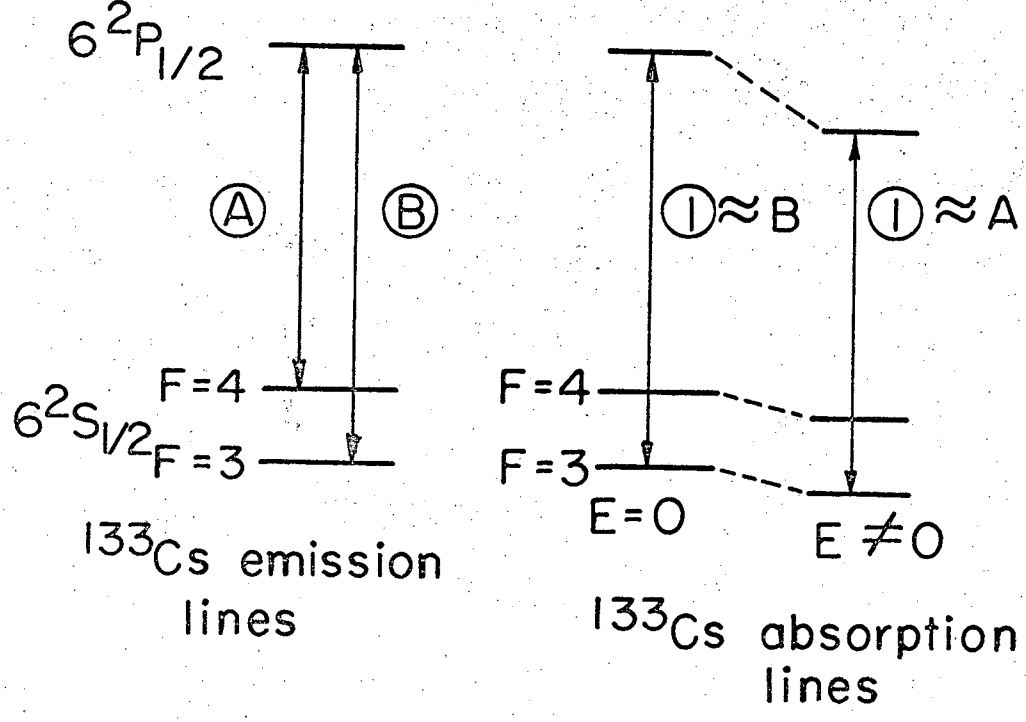
$6^2P_{1/2}$
A
B
F=4
$6^2S_{1/2}$ F=3
^{133}Cs emission lines
1 ≈ B
1 ≈ A
F=4
F=3
E=0
E≠0
^{133}Cs absorption lines
XBL673-2405

Fig. 16

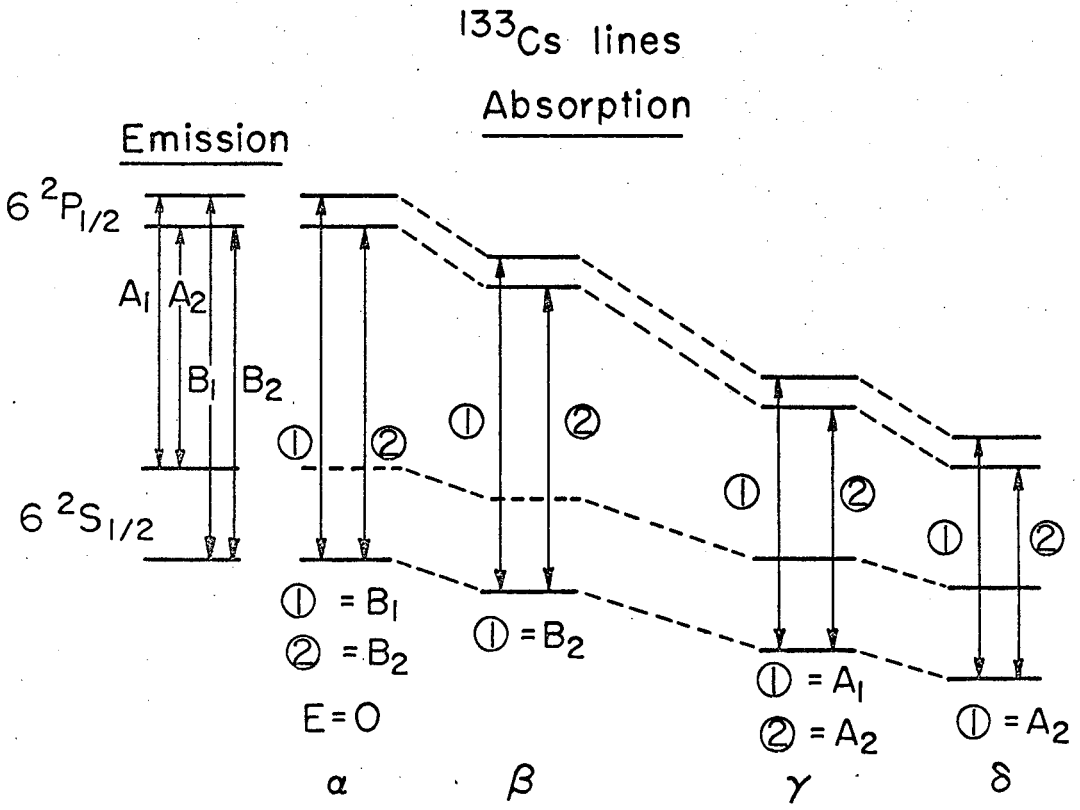

XBL673-2406

Fig. 17